









BRIEF DEFINITIVE REPORT

Metabolic bifunctionality of Rv0812 couples folate and peptidoglycan biosynthesis in *Mycobacterium tuberculosis*

Katherine A. Black^{1*} , Lijun Duan^{2*} , Lungelo Mandyoli² , Bruna P. Selbach¹ , Weizhen Xu¹ , Sabine Ehrt¹ , James C. Sacchettini² , and Kyu Y. Rhee¹ 

Comparative sequence analysis has enabled the annotation of millions of genes from organisms across the evolutionary tree. However, this approach has inherently biased the annotation of phylogenetically ubiquitous, rather than species-specific, functions. The ecologically unusual pathogen *Mycobacterium tuberculosis* (*Mtb*) has evolved in humans as its sole reservoir and emerged as the leading bacterial cause of death worldwide. However, the physiological factors that define *Mtb*'s pathogenicity are poorly understood. Here, we report the structure and function of a protein that is required for optimal in vitro fitness and bears homology to two distinct enzymes, Rv0812. Despite diversification of related orthologues into biochemically distinct enzyme families, *rv0812* encodes a single active site with aminodeoxychorismate lyase and D-amino acid transaminase activities. The mutual exclusivity of substrate occupancy in this active site mediates coupling between nucleic acid and cell wall biosynthesis, prioritizing PABA over D-Ala/D-Glu biosynthesis. This bifunctionality reveals a novel, enzymatically encoded fail-safe mechanism that may help *Mtb* and other bacteria couple replication and division.

Introduction

Despite Koch's discovery of *Mycobacterium tuberculosis* (*Mtb*) as the causative agent of tuberculosis (TB) over 130 yr ago, TB remains the leading cause of death due to infectious disease and has emerged as the leading cause of death due to antibiotic resistance (World Health Organization, 2020). Surprisingly, knowledge of *Mtb*-specific physiology remains incomplete. High-throughput sequencing technologies have helped to overcome this barrier (Cole et al., 1998; Saghatelian and Cravatt, 2005); however, it is estimated that approximately one third to one half of all *Mtb* genes lack a functional annotation, are potentially misannotated, or encode noncanonical activities beyond their predicted functions (Hanson et al., 2009).

Current bioinformatic sequence annotations, to a great extent, are based on sequence homology. These methods derive their utility from phylogenetically conserved structure–function relationships. While powerful, these methods are associated with an underappreciated bias favoring the annotation of evolutionarily invariant functions, leaving the most specific features of a given organism's physiology undefined (Cole et al., 1998; Lechartier et al., 2014). This bias is amplified further by its extension to genes exhibiting intermediate degrees of sequence conservation, where annotations of ancestral over

species-specific functions are favored, and when functions are identified, they are often restricted to a general class level.

Here, we investigated the function of *rv0812*, a gene that was predicted to be essential for in vitro growth of *Mtb* and found to be upregulated within the lungs of infected mice, but that bears homology to two biochemically distinct enzymes (DeJesus and Ioerger, 2013; DeJesus et al., 2017b; Dubnau et al., 2005; Griffin et al., 2011; Zhang et al., 2012). Bioinformatic sequence analysis identified Rv0812 as a member of the type IV family of pyridoxyl-5'-phosphate (PLP)-dependent enzymes (PLPDEs), with nearly equivalent degrees of homology to bacterial amino-transferases involved in synthesis of cell wall-associated D-amino acids and enzymes involved in the synthesis of the folate precursor para-aminobenzoic acid (PABA; Cole et al., 1998; Kapopoulou et al., 2011; Lew et al., 2011; Pruitt et al., 2007; Wattam et al., 2014). Previous work implicated a role for Rv0812 in the latter (Chim et al., 2011; Thiede et al., 2016). Using a combination of biochemistry, metabolomics, structural biology, and chemical genetics, we demonstrate that Rv0812 catalyzes two enzymatic reactions in biochemically unrelated pathways. One is as an aminodeoxychorismate (ADC) lyase (ADCL) involved in folate biosynthesis. The other is as a D-amino acid

¹Weill Cornell Medicine, New York, NY; ²Texas A&M University, College Station, TX.

*K.A. Black and L. Duan contributed equally to this paper; Correspondence to Kyu Y. Rhee: kyr9001@med.cornell.edu; James C. Sacchettini: sacchett@tamu.edu.

© 2021 Black et al. This article is available under a Creative Commons License (Attribution 4.0 International, as described at <https://creativecommons.org/licenses/by/4.0/>).

transaminase (DAAT) involved in peptidoglycan (PG) biosynthesis. All reported ADCLs and DAATs have been found to be encoded by separate genes (Jhee et al., 2000; Mehta and Christen, 2000; Miles, 1985). The bifunctionality of Rv0812 suggests that *Mtb* has encoded one enzyme with both activities to mechanistically buffer against the competing metabolic demands of nucleic acid and cell wall biosynthesis in a manner that may ensure the orderly progression of *Mtb* replication and division.

Results and discussion

Biochemical characterization of recombinant Rv0812

Comparative sequence analysis annotates Rv0812 as a type IV PLPDE (Cole et al., 1998). PLP, the biologically active form of vitamin B6, is an enzymatic cofactor used by one of the most diverse superfamilies of enzymes and is involved in the catalysis of a wide range of transamination, decarboxylation, deamination, and racemization reactions (Christen and Mehta, 2001). The type IV family of PLPDEs is distinguished by a stereochemically conserved active site architecture that promotes re-face rather than si-face proton transfer relative to the C4' of the planar pi system of the cofactor (Jhee et al., 2000; Martínez del Pozo et al., 1989a; Sugio et al., 1995; Yoshimura et al., 1993). Annotated members of the type IV family include ADCL, DAAT, branched chain amino acid transaminase, and R-stereospecific amine transaminase (Percudani and Peracchi, 2009), each of which appears to have divergently evolved distinct substrate and reaction specificities.

In contrast to most type IV PLPDEs, Rv0812 exhibits equivalent degrees of sequence homology to both ADCLs and DAATs. Published work has implicated Rv0812 in each role (Chim et al., 2011; DeJesus et al., 2017a; Kieser et al., 2015; Thiede et al., 2016; Xu et al., 2017). We sought to resolve this ambiguity by characterizing the in vitro activity of purified recombinant Rv0812. Consistent with previous phenotypic studies of a Rv0812 transposon mutant and biochemical assays of a purified preparation of recombinant Rv0812, we first confirmed Rv0812's enzymatic activity as an ADCL (Chim et al., 2011). Owing to the intrinsic chemical instability of the substrate ADC, which precluded determination of absolute kinetic parameters, we assayed for ADCL activity using a published coupled assay in which ADC was generated in situ through the addition of chorismate to purified *Escherichia coli* ADC synthase (*pabB*), and ADCL activity was detected by spectrophotometric monitoring of pyruvate production using lactate dehydrogenase (LDH; Ye et al., 1990). We observed activity levels similar to those reported for the *E. coli* and *Plasmodium falciparum* ADCL enzymes, with Rv0812 catalyzing ADC turnover at 1.9 s^{-1} compared with 15 and 5 s^{-1} for the orthologues from *E. coli* and *P. falciparum*, respectively (Fig. 1 E; Jhee et al., 2000; Magnani et al., 2013).

Multiple transposon mutagenesis-based screens have separately identified Rv0812 in focused studies of *Mtb* peptidoglycan metabolism (DeJesus et al., 2017a; Kieser et al., 2015; Xu et al., 2017). In addition, a recent study in *Mycobacterium smegmatis* discovered a shunt from D-Glu to D-Ala in an *alr* insertion mutant, prompting the proposal of an alternative transaminase

(Marshall et al., 2017). Further studies revealed that the Rv0812 orthologue, MSMEG_5795, encoded a DAAT activity capable of restoring growth to strains deleted in either glutamate racemase (ΔmurI) or alanine racemase (Δalr) when overexpressed (Mortuza et al., 2018). We therefore directly assayed *Mtb* Rv0812 for in vitro activity as a DAAT and discovered a time- and enzyme-dependent stereospecific turnover of D-Ala and D-Glu that could also be observed in the presence of a mycobacterial small-molecule extract containing hundreds of potentially competing substrates (Fig. 1, A and D; de Carvalho et al., 2010). Kinetic studies revealed that Rv0812's DAAT activity is strictly restricted to D-Ala and D-Glu, as a substrate mix containing α -ketoglutarate (AKG) and a combination of all other D-amino acids showed minimal D-Glu production over time (Fig. S1 A).

To determine the catalytic efficiency of this activity, we determined steady-state kinetic parameters for D-Ala (K_M [Michaelis constant] and k_{cat} [turnover number] $7.3 \pm 1.1 \text{ mM}$ and 1.46 s^{-1} , respectively; Fig. S1 B) and D-Glu (K_M and k_{cat} $0.24 \pm 0.05 \text{ mM}$ and 0.252 s^{-1} , respectively; Fig. S1 C). These values are comparable to those reported for the DAAT from the *Bacillus sp.* YM-1 strain (K_M and k_{cat} for D-Ala: $48 \pm 12 \text{ mM}$ and 129.6 s^{-1} ; K_M and k_{cat} for D-Glu: $1.2 \pm 0.2 \text{ mM}$ and 4.3 s^{-1} , respectively), which exhibits weaker substrate affinities but higher turnover rates (Fig. 1 E; Bhatia et al., 1993). The *M. smegmatis* homologue of Rv0812, MSMEG_5795 (70% identity), similarly exhibited a comparable kinetic profile (Fig. 1 E; Mortuza et al., 2018). In contrast, a comparison of specificity constants (k_{cat}/K_M) revealed a preference of Rv0812 for D-Glu over D-Ala (1 vs. 0.2) while the *Bacillus* DAAT exhibited similar values for both substrates (2.7 vs. 3.6).

Substrate competition experiments were conducted to further elucidate the physiological substrate preferences of Rv0812 under conditions in which both ADCL and DAAT substrates were present. This analysis demonstrated that the catalytic efficiency of Rv0812's ADCL activity was reduced by ~50% in the presence of saturating concentrations of D-Ala or D-Glu (Fig. S1, D and E). Both substrates mediated this inhibition in a competitive manner, as their presence increased K_M for ADC (Fig. S1 D) without affecting the turnover rate (Fig. S1 E). Consistent with the higher binding affinity of Rv0812 for D-Glu over D-Ala, the presence of D-Glu imparted a more dramatic increase in Rv0812's K_M for ADC (Fig. S1 D). This is further supported by prior reports of D-Glu-mediated ADCL inhibition in the absence of keto-acids (Magnani et al., 2013). Interestingly, in the reverse competition experiments, we found that while ADC similarly acted as a competitive inhibitor of Rv0812's DAAT activity with D-Ala as a substrate, its presence had little impact on Rv0812's kinetic parameters for reactions with D-Glu as the substrate (Fig. S1, F and G).

Structural characterization of Rv0812

To elucidate the structural basis of Rv0812's enzymatic bifunctionality, we determined the x-ray crystal structure of recombinant Rv0812 at $2.4\text{-}\text{\AA}$ resolution. Crystals of apo-Rv0812 belonged to the primitive monoclinic space group $P2_1$ with two molecules in the asymmetric unit, consistent with the behavior of Rv0812 on size exclusion chromatography and of other ADCLs

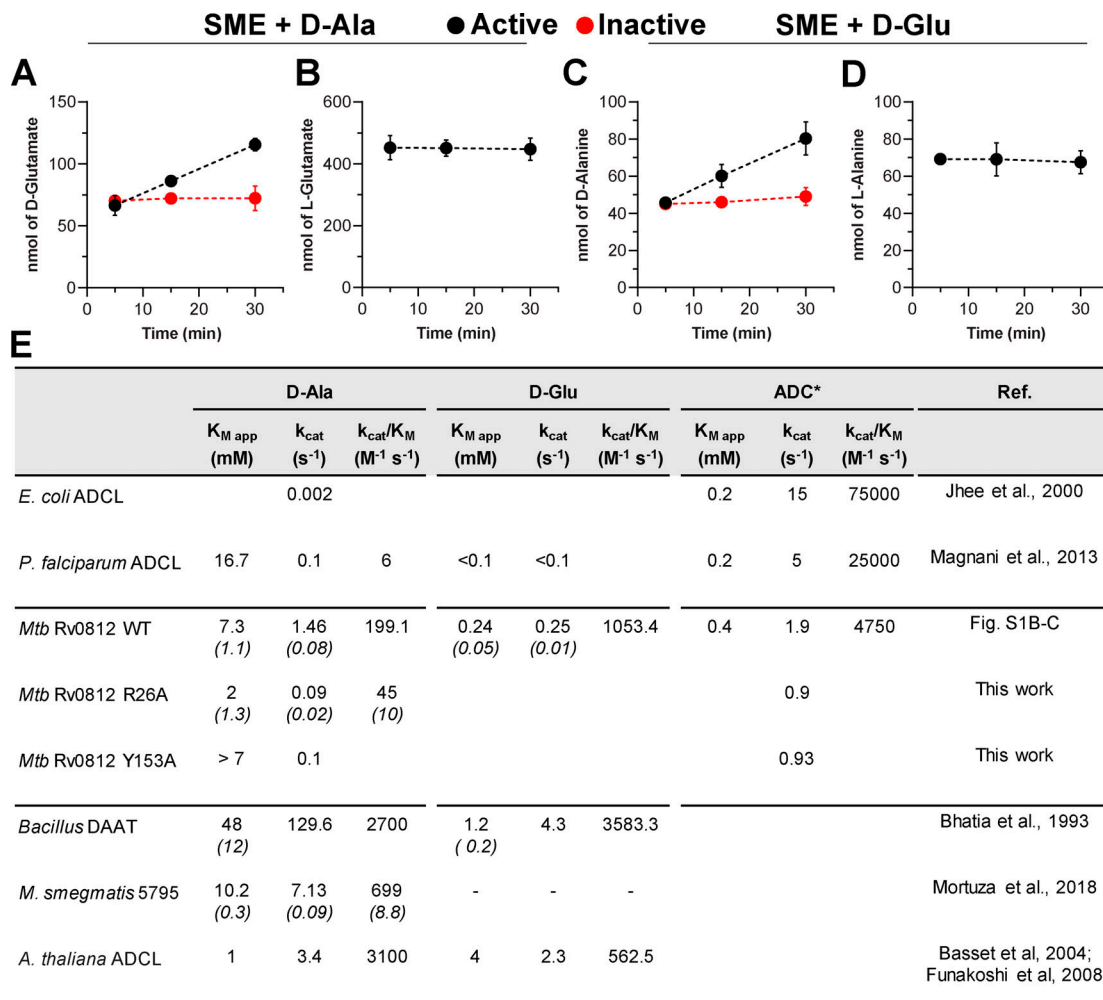


Figure 1. Rv0812 is a bifunctional enzyme with DAAT and ADCL activities. ABMP experiments revealed the DAAT activity of Rv0812. **(A–D)** Reactions (150 μl) containing 75 μl SME substrate, 50 μM PLP, 1 mM D-Ala (A and B) or D-Glu (C and D), and 5 μM Rv0812 were monitored by quenching aliquots at various time points for LC-MS analysis. Accumulation of D-Ala or D-Glu was dependent on the presence of active enzyme and had no impact on the concentration of L-enantiomers present in the SME. **(E)** Kinetic parameters for *Mtb* Rv0812 WT and variants were determined with pure substrates and compared with those of known DAAT and ADCL enzymes. SDs are shown inside parentheses in italics. (Kinetic parameters with ADC as substrate are reported as rough approximations, as ADC instability prevents well-defined substrate concentrations and, thus, accurate kinetic determination.) SDs were obtained from at least three independent experiments.

and DAATs that are functional as homodimers in solution (Table S1; Martínez del Pozo et al., 1989b; Padmanabhan et al., 2009; Ye et al., 1990). Crystals of PLP-bound Rv0812 were similarly found to belong to the $P2_1$ space group, with four molecules—composed of two homodimers, AB and CD—in the asymmetric unit (Table S1). Molecular replacement using the type IV PLPDE CpuTA1 from *Curtobacterium pusillum* (Protein Data Bank [PDB] accession no. 5K3W) was used to solve and refine the structure of apo-Rv0812. The refined apo-structure was used to solve the structure of Rv0812 with PLP. There was clear electron density extending from the sidechain of Lys149 (Fig. 2 C), predicted to form the Schiff base with PLP. PLP was fit into the corresponding electron density and it was refined with good stereochemistry for all four molecules found in the asymmetric unit (Fig. 2 C). Residues common to type IV PLPDEs and involved in PLP binding, including His47, Arg50, Tyr153, Glu182, and Ser253, were similarly observed (Fig. 2 C; Marchler-Bauer et al., 2017),

although residues neighboring the active site differed from those in other PLP-dependent enzymes (Fig. 2 D).

Superimposing the PLP-bound structure of Rv0812 onto representative PLP-bound DAAT and ADCL structures, we identified structural features that distinguished the Rv0812 active site from that of the DAAT from the *Bacillus* sp. YM-1 strain (BsDAAT; Peisach et al., 1998) and ADCL from *Pseudomonas aeruginosa* (PaADCL, PDB: 2Y4R; O'Rourke et al., 2011). BsDAAT and PaADCL share 23% and 27% sequence identity with Rv0812, respectively. Overlaying all three active sites, we noted a conserved set of core catalytic residues—K149/K145/K140, E182/E177/E173, and R50/R50/R46—in Rv0812, BsDAAT, and PaADCL, respectively (Fig. 2 D); however, there were unique features of the Rv0812 active site that help explain its dual specificity. The active sites of BsDAAT and PaADCL both include a long loop of substrate-interacting residues that extend from the opposing subunit (Fig. 2 B). In BsDAAT, two residues in this loop—Arg98*

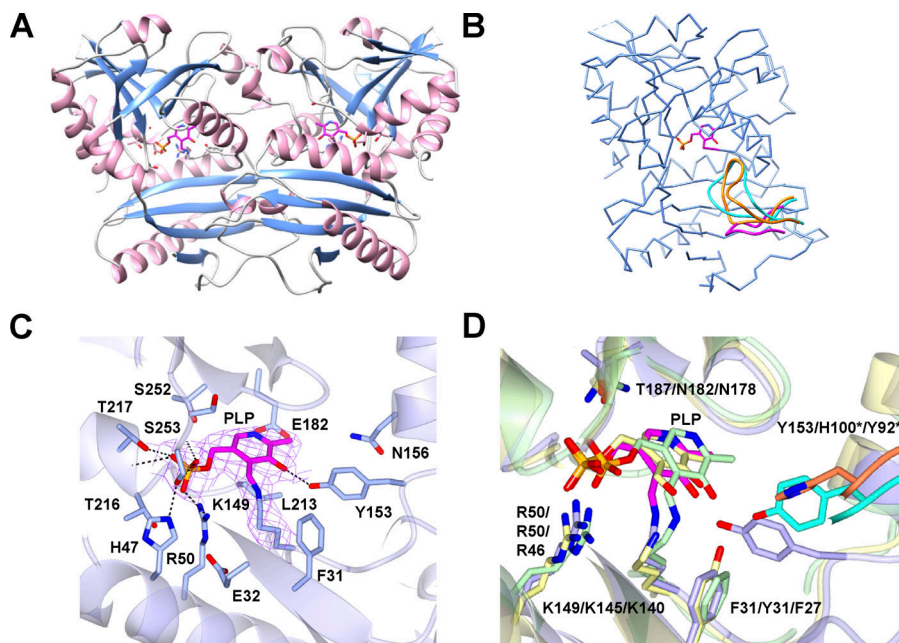


Figure 2. Structural characterization of Rv0812 reveals the basis for dual ADCL and DAAT activities. (A) Ribbon diagram of PLP-bound dimer (loops in gray, α-helices in pink, and β-sheets in light blue; panels A–D display the PLP molecule in magenta). (C) Side chains of PLP-neighboring residues within 5 Å are shown. (B and D) Structural comparison to BsDAAT and PaADCL. A shortened loop in Rv0812 (magenta) prevents interaction with the partner subunit active site, as in BsDAAT (orange) and PaADCL (cyan). (D) Active site comparison of PLP-Rv0812 (purple), PLP-bound BsDAAT (yellow), and PaADCL (green), with residues labeled as Rv0812/BsDAAT/PaADCL. H-bonds formed between Rv0812 and PLP (C) are shown with dashed lines, and the [(2Fo) - (Fc)] electron density map, contoured at 1.2σ, of PLP and Lys149 (C) is shown as chicken wire.

and His100*—close to the –OH of PLP, have been proposed to comprise a carboxylate trap (Peisach et al., 1998), required for correct positioning of incoming substrates. PaADCL also contains a 17-residue long loop, structurally similar to that of BsDAAT, but which is involved in stabilizing PLP-OH via a Tyr92* residue (O'Rourke et al., 2011). In contrast, Rv0812 encodes a much shorter loop that consists of only nine residues (L7: Arg95*–Pro103*), none of which appear to interact directly with substrates for either reaction (Fig. 2 B).

In light of this difference, we determined the structure of Rv0812 bound to its DAAT products in order to elucidate the structural basis of substrate binding by Rv0812. Rv0812 crystals produced after incubation with PLP and D-Glu were isomorphous with the PLP-containing crystals (Table S1) and contained electron density corresponding to pyridoxamine 5'-phosphate (PMP) and AKG in the active site, allowing the cofactor and product to be manually built in Emsley and Cowtan (2004). The PMP-AKG bound structure revealed that Arg98* in BsDAAT (Figs. 2 C and S1 N), which formed H-bonds and salt bridges with the AKG C5 (2.7 Å) and D-Ala carboxylates (3.3 Å, 3.4 Å), corresponding to Arg26* in Rv0812, while Arg115 and Arg185 donated H-bonds (2.4 Å, 2.8 Å) to the AKG C5 carboxylate, and Arg115 (2.7 Å) and Thr255 (3.0 Å) stabilized the AKG C1 carboxylate (Fig. S1, J and K). These interactions serve to identify a structurally distinct, but functionally analogous, carboxylate trap in Rv0812, while allowing for potentially broader substrate specificity (Figs. 2 and S1, J and N).

Experimental efforts to obtain crystals of Rv0812 bound to PABA were unsuccessful; however, in silico modeling of Rv0812 using the structure of PaADCL enabled manual docking of ADC into the AKG binding site of the PMP-AKG bound structure. Notwithstanding known limitations of energy minimization-based docking studies (that include protein structure rigidity and the absence of coordinating water molecules), this model revealed a series of ADC-coordinating residues that notably

included the carboxylate trap residues Arg26*, Arg115, and Arg185, which appear positioned to stabilize the C9 carboxylate of ADC through a network of H-bonds and salt bridges (2.8 Å, 3.3 Å, 3.1 Å), while Arg 115 (2.3 Å), Ser252 (2.7 Å), and Thr255 (2.5 Å) appear within H-bonding distance of the C5 carboxylate of ADC, and Arg26* and Thr33 appear within H-bonding distance of the oxygen next to the C1 olefin (2.3 Å) and amino group (3.1 Å) of ADC, respectively (Fig. S1 L). An overlay of the Rv0812-AKG complex structure with that of PaADCL conversely revealed a Tyr residue (Tyr22*) at the position corresponding to Arg26*, but Tyr22 was nearly 5 Å away from the AKG C5 carboxylate (Fig. S1 P).

Interestingly, ADCL enzymes from *E. coli* and *P. falciparum*, both of which contain the conserved Y22 residue, have previously been shown to act on D-Ala (Jhee et al., 2000; Magnani et al., 2013). Due to their extremely low efficiencies with D-Ala, however, these activities were proposed to be moonlighting functions derived from a shared ancestral active site. The turnover rate of D-Ala transamination by the *E. coli* ADCL was specifically found to be 700-fold lower than that of Rv0812, and catalytic efficiency of *P. falciparum* ADCL was more than 30-fold less than that of Rv0812 (Fig. 1 E). Comparison of Rv0812's kinetic parameters with those of Y22-containing ADCL enzymes with apparent moonlighting DAAT activities thus supports a critical role for the R26* residue in mediating physiological levels of DAAT activity.

Putting the foregoing structural model to test, we generated and characterized the catalytic activity of a purified recombinant mutein of Rv0812 harboring a nonconservative substitution (R26A*) in a key residue of its putative carboxylate trap. Consistent with its predicted interaction with substrates of both its DAAT and ADCL activities, we observed reproducible reductions in the apparent turnover rates (k_{cat}) of both reactions in the R26A mutant compared with WT protein (Fig. S1 H). DAAT activity of the R26A variant exhibited a greater impact on k_{cat}

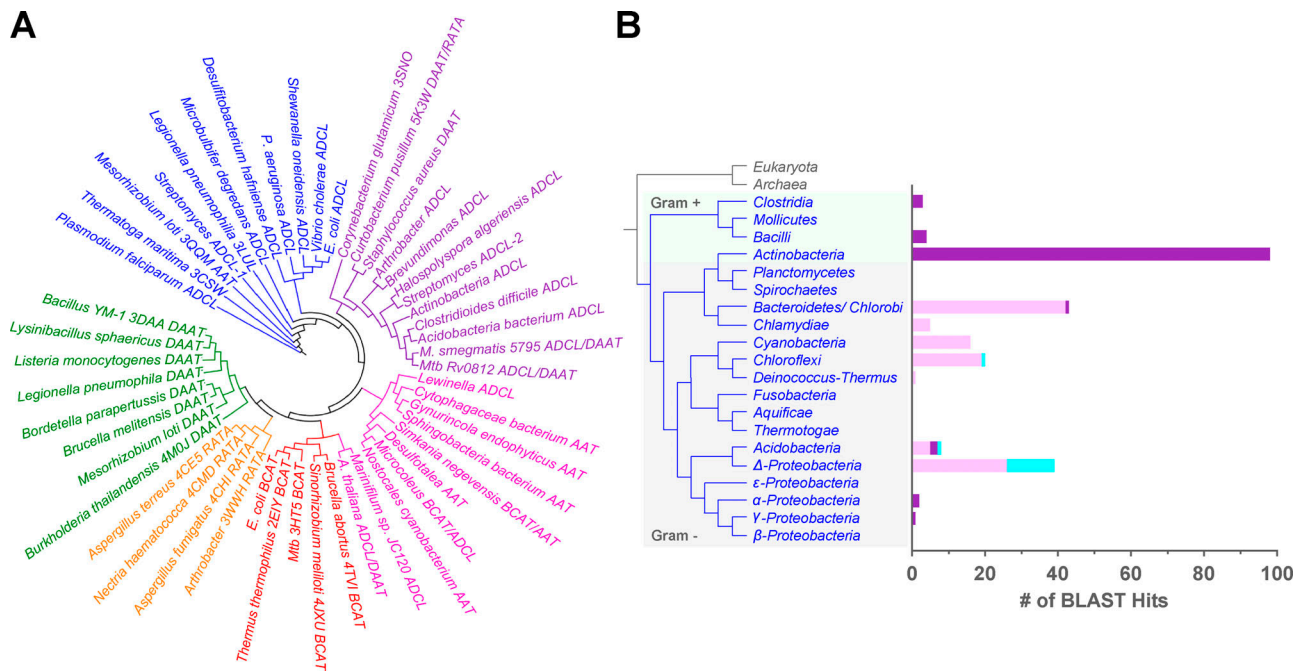


Figure 3. Rv0812 characterization enables discovery of new subgroups within the type IV PLPDE family. (A) The cladogram of type IV PLPDEs shows separation into distinct subgroups with different functions. ADCL-, DAAT-, branched chain amino acid transaminase-, and R-stereospecific amine transaminase-like sequences are colored in blue, green, red, and orange, respectively. Rv0812-like sequences were discovered by BLAST searches against each bacterial phylum shown in B and filtered to select only sequences containing Arg26. Phylogenetic analysis resulted in separation of Rv0812 orthologues into two distinct clades. Those with high similarity to Rv0812 are shown in purple (Clade I), while those with lower similarity are in pink (Clade II). National Center for Biotechnology Information annotations are provided and PDB accession nos. are shown for those with solved structures. Sequences were aligned using ClustalW2, and the tree was created using the neighbor-joining method with BLOSUM62. **(B)** The distribution and frequency of Rv0812-like orthologues across bacterial phyla was estimated by plotting the number of filtered BLAST hits (of 100 maximum) per phylum (total bar height). The number of sequences that clustered to Clade I is shown in purple, while the number of sequences in Clade II or neither group are shown in pink and cyan, respectively.

($0.09 \pm 0.2 \text{ s}^{-1}$) over K_M , D-Ala ($2 \pm 1.3 \text{ mM}$), suggesting a mechanistic role for the carboxylate trap in formation of a productive enzyme-substrate complex (Fig. 1 E). Furthermore, the heightened impact of the R26A substitution on the DAAT activity of Rv0812, specifically, supports the notion that it is responsible for boosting DAAT activity to the extent that it is physiologically relevant.

Bioinformatic reanalysis of Rv0812 phylogeny

The structural identification of active site residues associated with the dual ADCL/DAAT activities of Rv0812 prompted a bioinformatic search for additional bifunctional orthologues (Marchler-Bauer et al., 2017). This resulted in the discovery of orthologous sequences containing the Arg26 residue across various bacterial phyla. A phylogenetic sequence analysis of type IV PLPDEs that included both ADCL and DAAT-like sequences further revealed that Rv0812 orthologues formed two distinct and novel clades. The clade containing Rv0812 (Clade I) clustered with a handful of annotated ADCL-like sequences but away from the majority of canonical ADCLs, while the second clade (Clade II) appeared to have more similarity to transaminase subfamilies within type IV PLPDEs (Fig. 3 A; Jhee et al., 2000; O'Rourke et al., 2011). Phylogenetic mapping across bacterial phyla further revealed that the majority of Clade I orthologues were found in gram-positive species, while Clade II orthologues were only found in gram-negative species (Fig. 3 B), suggesting

the divergent evolution of a distinct, but yet-to-be determined, activity.

Previous analyses had identified two separate subclasses of ADCL-like enzymes based on the subunit contributions of the active site Tyr92/Tyr153 residue, with one subclass deriving its active site Tyr residue from the same subunit forming the active site (Position I) and the other subclass contributing the active site Tyr to the opposite protomeric subunit (Position II; O'Rourke et al., 2011). PaADCL belongs to the former subclass, while Rv0812 is a member of the latter. Surprisingly, the two ADCL clusters observed in our analysis did not conform to this classification, as members of the Position II subclass were observed in both clusters, though all sequences in the Rv0812 cluster belonged to the Position II subclass (Waterhouse et al., 2009). We found instead that all Rv0812-like, ADCL-like sequences encoded an Arg (R26*) rather than Tyr (Y22*) at the equivalent position, in addition to several other conserved sequence differences (Fig. S2). The Rv0812-containing cluster thus appears to constitute a novel group of the Position II subclass, with sequences that share greater active site similarity to DAATs.

Awaiting future studies of this nascent subclass of bifunctional ADCL-like sequences, studies of the ADCL from *Arabidopsis thaliana*, which encodes the same conserved active site residues as Rv0812 (Fig. S2 A), have separately reported evidence of ADCL activity in one study and DAAT activity in

another (Basset et al., 2004; Funakoshi et al., 2008). Moreover, superpositioning the active site of Rv0812 with that of an in silico model of ADCL/DAAT from *A. thaliana* (Fig. S2 B) further revealed a high degree (eight of 12 residues) of conservation of residues lining the cofactor binding site, while the spatial position of the catalytically important Arg26* of Rv0812 differed from that of Arg104* in the *A. thaliana* structure by less than 1.1 Å among all nearby main chain atoms (Fig. S2 C).

It is similarly interesting to note the presence of two annotated ADCL (*pabC*)-like sequences in the *Streptomyces* genome (Zhang et al., 2009). The canonical PabC-1 sequence, encoded by a gene located near *pabAB*, shows the conservation of the canonical ADCL Y22 and N236 residues, while the PabC-2 sequence, phylogenetically clustered with Rv0812, does not. It is unknown whether PabC-1 and -2 exhibited DAAT activity, but the unusual occurrence of two ADCL sequences in the genome and differences in their active site conservation suggest an additional DAAT function for PabC-2, rather than redundancy.

Physiological characterization of Rv0812

Phylogenetic predictions notwithstanding, we sought evidence of a physiological linkage between these two biochemically distinct activities. To do so, we generated a precise isogenic deletion of Rv0812. Consistent with previous reports of an Δ Rv0812 mutant in *H37Ra* and a transposon insertion mutant in *H37Rv*, Δ Rv0812 *Mtb* exhibited a growth defect in liquid culture that could be corrected by expression of an extragenic copy of the WT allele or chemical addition of PABA to the culture medium (Fig. S1 I; Thiede et al., 2016). Comparative metabolic profiling further revealed a marked and selective accumulation of ADC, while the levels of PABA and downstream intermediates of folate biosynthesis were markedly depleted compared with WT and Rv0812 reconstituted strains (Fig. 4 A). These changes were further linked to a >10-fold increase in susceptibility to the antifolate, para-aminosalicylic acid (PAS; Fig. S3 B). These results establish a nonredundant, physiological role for Rv0812 in de novo folate biosynthesis.

Seeking physiological evidence of DAAT activity in vivo, we performed metabolomic profiling of WT, Δ Rv0812, and Δ Rv0812::Rv0812 strains incubated in the presence of either exogenous D-Ala or D-Glu. Δ Rv0812 *Mtb* exhibited a selective and genetically complementable defect in D-Glu pools, but not D-Ala pools (Fig. 4 A). Incubation with exogenous D-Ala further revealed linked Rv0812-dependent increases in L-Ala, (D-Ala)₂, and D-Glu (Figs. 4 B and S3 G), whereas reciprocal effects of D-Glu supplementation were not observed (Figs. 4 C and S3 H). These findings suggest that under the conditions tested, Rv0812 operates in the direction D-Glu synthesis. This directionality and physiological role are consistent with the nearly sixfold higher k_{cat} of Rv0812 for D-Ala than D-Glu as a substrate, near equivalent k_{cat} of *Mtb* alanine racemase (Alr) for D- and L-Ala as substrates, and general kinetic preference of bacterial *Mtb* glutamate racemase (MurI) enzymes for L-Glu over D-Glu. Moreover, where determined, D-Glu pools have been reported to be ~10-fold lower than L-Glu pools, suggesting that D-Glu synthesis is tightly regulated at low levels, whereas L- and D-Ala pools are maintained at near equal concentrations, consistent with

apparent equilibrium position—or ratio—of their k_{cat} s. To further validate our findings, we determined what, to our knowledge, are the first measurements of the effective aqueous intrabacterial concentrations of D-Ala and D-Glu (2.1 ± 1.01 and 0.15 ± 0.05 mM, respectively) and L-Ala and L-Glu (2.9 ± 1.65 and 21 ± 10 mM, respectively) in *Mtb*. These values and near unit ratio of forward and reverse reaction rates of *Mtb*'s Alr support a basal or failsafe role for Rv0812 in coupling D-Ala and D-Glu synthesis to one another—a finding physiologically supported by the selective defect in D-Glu pools observed in Rv0812-deficient strains. In addition, the apparent lack of D-Glu-induced changes in D-Ala pools may be explained by the nearly 39-fold-higher turnover rate of D-alanyl-D-alanine ligase (Ddl) than that of Rv0812 ($k_{cat} = 9.7 \text{ s}^{-1}$ and $k_{cat, \text{D-Glu}} = 0.252 \text{ s}^{-1}$ for Ddl and Rv0812, respectively; Prosser and de Carvalho, 2013c). These results nonetheless collectively demonstrate the physiological competency of the DAAT activity of Rv0812.

Given the reported positive or alleviating epistatic interactions of Rv0812 with several annotated genes of PG metabolism (DeJesus et al., 2017a; Kieser et al., 2015; Xu et al., 2017), we also sought to directly test the functional importance of the DAAT activity of Rv0812 in PG biosynthesis. To do so, we tested the susceptibility of Δ Rv0812 to D-cycloserine (DCS) and β -chloro-D-alanine (BCDA), two validated whole-cell active inhibitors of *Mtb* PG biosynthesis (David, 2001; Manning et al., 1974; Prosser and de Carvalho, 2013a). DCS is a clinically approved second-line TB drug whose mode of action is mediated by inhibition of Alr and Ddl (Prosser and de Carvalho, 2013b), while BCDA was recently shown to act as a whole cell-active, mechanism-based inhibitor of MurI (Prosser et al., 2016). Consistent with their established primary targets, we observed no difference in the minimum inhibitory concentration of either DCS or BCDA against Δ Rv0812 (Fig. S3, A and C). Following exposure to supra-MIC (minimum inhibitory concentration) levels, however, we noted that the Δ Rv0812 mutant exhibited an additional 1 log₁₀ loss of viability compared with either the WT or complemented strain for each compound, indicating an essential and specific role for the DAAT activity of Rv0812 in *Mtb* viability when Alr or MurI racemase activity is absent. We further showed that this enhanced susceptibility to DCS or BCDA could be rescued, in part, by the addition of exogenous D-Ala and D-Glu, or PABA, to the culture medium (Fig. 5, A and C). These results provide further physiological evidence of Rv0812's activity as a bidirectional DAAT.

Restoration of WT levels of susceptibility to either DCS or BCDA in Δ Rv0812 *Mtb* required the joint addition of exogenous D-Ala, D-Glu, and PABA (Fig. 5, A and C). Given the chemically and mechanistically distinct nature of DCS and BCDA and the fact that PABA alone did not cause any measurable degree of rescue from DCS or BCDA in WT *Mtb*, this requirement suggested that the increased susceptibility of Δ Rv0812 *Mtb* to both DCS and BCDA was due to a loss of both the DAAT and ADCL activities of Rv0812.

Interestingly, DCS exhibited a larger impact on Δ Rv0812 *Mtb* than BCDA. Recent work has shown that the antimycobacterial activity of DCS is mediated through the inhibition of multiple targets (de Chiara et al., 2020). We profiled the metabolomic impact of DCS on WT *Mtb* during the prelethal phase of

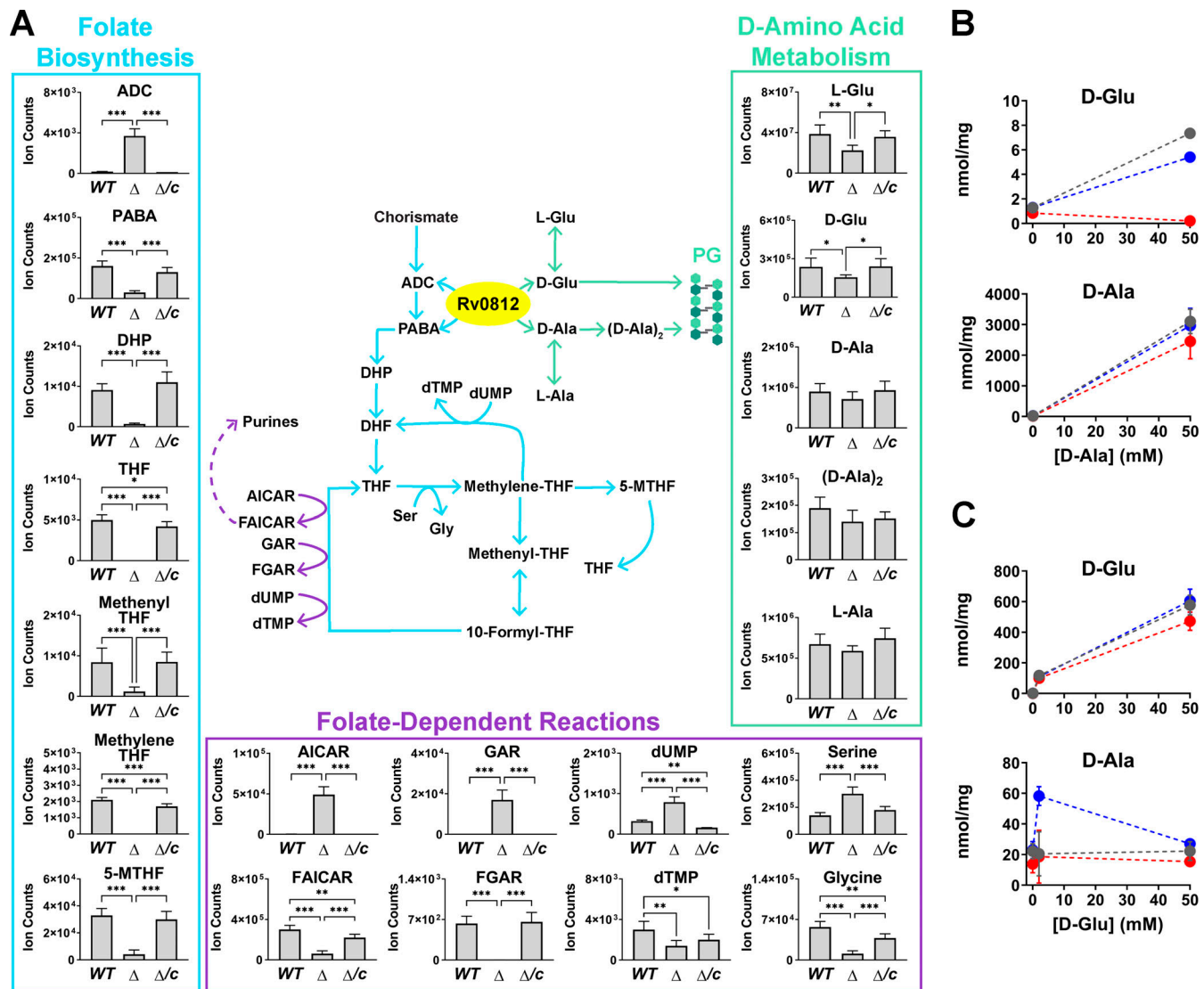


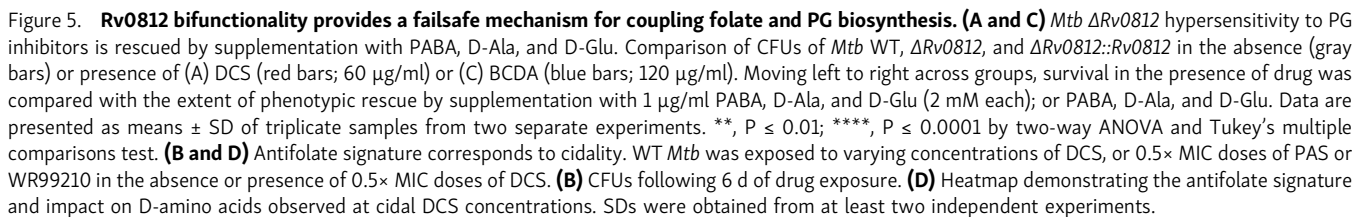
Figure 4. Rv0812 impacts *Mtb* folate and D-amino acid metabolism. (A) *Mtb* Δ Rv0812 is significantly impaired for folate biosynthesis and exhibits minor defects in D-amino acid metabolism. Intracellular metabolite abundance levels within *Mtb* WT, Δ Rv0812 (Δ), and Δ Rv0812::Rv0812 (Δ/c) strains grown in Sauton's media. Whereas the Δ Rv0812 strain displayed only minor deficiencies in D-amino acid levels (green), loss of Rv0812 conferred severe defects within folate biosynthesis (blue) and downstream folate-dependent reactions (purple). Data are presented as means \pm SD of triplicate samples from two separate experiments. *, $P \leq 0.05$; **, $P \leq 0.01$; ***, $P \leq 0.001$ by one-way ANOVA and Tukey's multiple comparisons test. (B and C) Rv0812 exhibits DAAT activity in vivo. Intracellular concentrations of D-Ala or D-Glu are shown in response to supplementation with 0, 2, and 50 mM D-Ala (B) or D-Glu (C). Intracellular metabolites from WT *Mtb* are shown in gray, while metabolites within Δ Rv0812 and Δ Rv0812::Rv0812 are shown in red and blue, respectively. SDs were obtained from at least two independent experiments. THF, 5, 6, 7, 8-tetrahydrofolate; DHP, dihydropterate; 5-MTHF, 5-methyl tetrahydrofolate; AICAR, 5-Amino-1-(5-phospho-beta-D-ribose)imidazole-4-carboxamide; dUMP, deoxyuridine monophosphate; dTMP, deoxythymidine monophosphate; FGAR, N2-Formyl-N1-(5-phospho-D-ribose)glycinamide.

treatment and discovered a specific impact on intermediates and downstream products of folate metabolism at bactericidal, but not bacteriostatic, concentrations (Fig. 5 D). We further observed that treatment of WT *Mtb* with subinhibitory concentrations of DCS combined with subinhibitory concentrations of either PAS or WR99210 (a whole-cell inhibitor of *Mtb*'s dihydrofolate reductase; Nixon et al., 2014) resulted in a $>5 \log_{10}$ reduction in *Mtb* viability (Fig. 5 B). This synergy suggests that the increased susceptibility of Δ Rv0812 *Mtb* to DCS than BCDA is due to its additional inhibition of *Mtb* folate biosynthesis. Moreover, this increased susceptibility reveals a previously

unrecognized biological coupling of PG and folate biosynthesis in *Mtb* that the enzymatic bifunctionality of Rv0812 appears poised to serve as an enzymatic failsafe defense.

Potential implications of a bifunctional ADCL/DAAT

Owing to their essentiality in bacteria and absence in humans, folate and PG biosynthesis pathways have served as highly validated antitubercular drug targets for decades (Gautam et al., 2011; Green and Matthews, 2007). Knowledge of specific physiological links between these two target pathways, however, has remained unaddressed. Like all cells, bacteria face the challenge



Our discovery of Rv0812 as a bifunctional ADCL and DAAT reveals a previously unrecognized metabolic coupling between nucleic acid and cell wall biosynthesis that appears to ensure prioritization of PABA production over D-Ala/D-Glu biosynthesis. This prioritization is evidenced by the phenotypic auxotrophy of Δ Rv0812 for PABA rather than D-Ala or D-Glu. Moreover, because both ADCL and DAAT activities are catalyzed by the same active site chemistry (Percudani and Peracchi, 2009), Rv0812 appears enzymatically poised to function as a metabolic toggle that alternates between ADCL and DAAT activity, prioritizing the former over the latter in response to substrate accumulation. From a structural perspective, this bifunctionality appears to have been selected for, in part, by the loss of conserved residues Y22, Y/H112, and N236 specific to ADCLs (Nakai et al., 2000; O'Rourke et al., 2011; Parsons et al., 2002). The reaction rates of its DAAT activity additionally indicate that Rv0812 kinetically favors the production of D-Glu five times more than D-Ala. This preference is further supported by the greater degree of Rv0812-dependent D-Glu accumulation in *Mtb*

The competition between ADCL and DAAT substrates for the active site of Rv0812 further reveals a new physiological link between nucleic acid and PG biosynthesis. This link is manifested by the increased vulnerability to DCS- or BCDA-mediated killing and the shared requirement for both PABA and D-Ala/D-Glu to restore WT levels of susceptibility, despite acting through a distinct set of molecular targets. This link is further reinforced by the marked, multi-log synergy of DCS and two mechanistically distinct antifolates when combined at subinhibitory concentrations against WT *Mtb*, as well as the heightened susceptibility of Δ Rv0812 *Mtb* to the dual impact of DCS on D-Ala and folate biosynthesis (Chakraborty et al., 2013; Nixon et al., 2014).

While powerful, an underappreciated limitation of homology-based gene annotations is their inherent bias toward evolutionarily invariant functions and limited ability to reveal functions related to more phylogenetically specific selective pressures. This is because conservation is an end product, rather than a driving force, of evolution. Yet organisms evolve their genomes in response to the specific selective pressures they encounter. Existing bioinformatic methods have therefore not sufficed to reveal the most distinguishing physiological features of a given organism. For pathogenic microbes, such as *Mtb*, such features correspond to a biologically ideal but untapped source of potential diagnostic biomarkers and drug targets. The discovery of ADCL-like enzymes with homology to Rv0812 across a wider range of bacteria suggests that coordination of bacterial growth and division may be a more broadly conserved, but previously unannotated, metabolic activity.

Materials and methods

Strain construction

The *rv0812* gene deletion mutant was constructed by allelic exchange via homologous recombination, as previously described (Gee et al., 2012), replacing the native copy of *rv0812* with a zeocin resistance cassette. Mutant candidates were isolated from Middlebrook 7H10 solid culture medium supplemented with 1 μ g/ml PABA and confirmed via Southern blot analysis. The *rv0812* complemented strain was constructed by reintroducing a copy of *rv0812* under the control of the *hsp60* promoter into the attL5 site of the *Mtb* genome. *Mtb* WT (H37Rv) and mutant strains were routinely grown in Sauton's medium with 0.04% tyloxapol, and, when necessary, zeocin and kanamycin were added to cultures at final concentrations of 25 μ g/ml and 20 μ g/ml, respectively.

Protein expression and purification

The sequence of the full-length Rv0812 gene was amplified from the *Mtb* H37Rv genome by PCR. The amplified gene was inserted into a pMCSG19B expression vector containing an N-terminal 6x-His tag using ligation-independent cloning sites (Eschenfeldt et al., 2009). The Rv0812:R26A and Rv0812:Y153A mutants were constructed by amplifying pMCSG19B-Rv0812 plasmids using the QuickChange II XL Site-Directed Mutagenesis Kit (Agilent Technologies). Plasmids were transformed into BL21(DE3) *E. coli* cells for protein expression. Cells with plasmids were grown at 37°C to an OD₆₀₀ of ~0.6–0.8 in Difco LB medium (Becton Dickinson) with 100 μ g/ml carbenicillin followed by induction with 500 μ M isopropyl β -D-1-thiogalactopyranoside and grown overnight at 18°C.

The sequence of the full-length EcPabB gene was amplified from a BL21(DE3) single colony by PCR. The amplified gene was inserted into the same plasmid as Rv0812 using the same method as described. The plasmids were transformed into BL21(DE3) *E. coli* cells for EcPabB expression. The cells with the plasmid were grown at 37°C to an OD₆₀₀ of ~0.6–0.8 in Difco LB medium with 100 μ g/ml carbenicillin followed by induction with 1 mM isopropyl β -D-1-thiogalactopyranoside and grown for 6.5 h at 37°C.

Cells were lysed via a Microfluidizer M-100P (Microfluidics) in lysis buffer (50 mM Tris [pH 7.5], 500 mM NaCl, 10% glycerol, 25 mM imidazole, 2 mM 2-mercaptoethanol, 1 mM PMSF, 10 μ g/ml DNase, and 2 mM MgCl₂) and centrifuged at 27,216 \times g for 1 h. The supernatant was purified over a nickel column with a 0–500-mM imidazole gradient, followed by size-exclusion chromatography using elution buffer (25 mM Tris [pH 7.5], 100 mM NaCl, 10% glycerol, 2 mM dithiothreitol). The proteins were >95% pure, as observed by SDS-PAGE, and were concentrated to 5 mg/ml, flash frozen, and stored in elution buffer at –80°C. Protein concentrations were determined by measuring A₂₈₀ using a NanoDrop 2000 UV-visible spectrophotometer (Thermo Fisher Scientific) using extinction coefficients of 37,930 M^{–1}cm^{–1} and 56,755 M^{–1}cm^{–1} for *Mtb* Rv0812 and EcPabB, respectively.

Activity-based metabolomic profiling (ABMP)

Mycobacterium bovis Bacillus Calmette-Guerin was grown in 7H9 medium supplemented with 0.2% glycerol, 0.5% BSA, 0.2% dextrose, and 0.085% NaCl. A 9-liter culture grown to OD_{580 nm} of 1.0 was harvested by centrifugation, and the resulting pellet was resuspended in 100 ml of an acetonitrile (ACN):methanol:H₂O (40:40:20) solution. Cells were lysed using an Emulsiflex C5 high-pressure homogenizer (Avestin) and centrifuged for 20 min at 20,000 \times g. Soluble extract was lyophilized and resuspended in 10 ml 25 mM Tris-HCl (pH 7.4), yielding the final small-molecule extract (SME).

For ABMP analysis, 150- μ l reactions containing 75 μ l SME and 5 μ M purified recombinant Rv0812 (active or heat killed for 15 min at 95°C) were incubated in 100 mM Tris-HCl (pH 8.5) at 37°C in the presence of 50 μ M PLP and 1 mM D-Ala or D-Glu. At indicated time points, reaction aliquots were quenched with cold ACN containing 0.2% formic acid for a final concentration of 80% quenching solution. After centrifugation at 20,000 \times g for 10 min, the resulting supernatant was separated from insoluble material and stored at 4°C for liquid chromatography-mass spectrometry (LC-MS) analysis.

Mass spectrometry

For separation and detection of metabolites, LC-MS analysis was conducted using an Agilent 1200 LC system containing a Cogent Diamond Hydride Type C silica column (150 mm \times 2.1 mm; Microsolv Technologies) coupled to an Agilent Accurate Mass 6220 TOF as described (Eoh and Rhee, 2013). The mobile phase consisted of solvent A (double-distilled H₂O with 0.2% formic acid) and solvent B (ACN with 0.2% formic acid) at a flow rate of 0.4 ml/min with the following gradient: 0–2 min, 85% B; 3–5 min, 80% B; 6–7 min, 75% B; 8–9 min, 70% B; 10–11.1 min, 50% B; 11.1–14 min, 20% B; and 14.1–24 min, 5% B; followed by a 10-min equilibration period at 85% solvent B before injection of the next sample. Dynamic mass axis calibration was accomplished by continuous infusion of a reference mass solution. Electrospray ionization capillary and fragmentor voltages were set at 3,500 V and 135 V, respectively. The nebulizer pressure was set to 40 psig and nitrogen drying gas was maintained at 250°C, set to a flow rate of 10 liter/min. The MS acquisition rate was 1.5 spectra/s and m/z data ranging from 50 to 1,700 was stored. Data

were analyzed using Profinder B.08.00 software, and ions were assigned as specific metabolites based on mass accuracy within 5 ppm and retention times within 1 min of those determined for chemical standards.

Enzymatic activity assays

Kinetic measurements of Rv0812's transaminase activity were obtained by means of two distinct assays, according to the substrate being consumed in the reaction. An LC-MS-based assay was used for kinetic analysis using D-Glu as the substrate. Reactions (200 μ l) contained 5 mM MgCl₂, 5 mM pyruvate, 50 μ M PLP, 0.25 μ M WT-Rv0812, and varying concentrations of D-Glu (50 μ M to 10 mM) in 100 mM Tris (pH 8.5). At indicated time points, reaction aliquots were quenched with cold ACN containing 0.2% formic acid for a final concentration of 80% quenching solution. After centrifugation at 20,000 \times g for 10 min, the resulting supernatant was separated from insoluble material and stored at 4°C for LC-MS analysis.

The kinetic parameters of Rv0812's transaminase activity, using D-Ala as a substrate, were determined by using an LDH-coupled assay. Reactions (200 μ l) were performed at 25°C in 100 mM Tris (pH 8.5) containing 5 mM MgCl₂, 5 mM AKG, 5 U/ml LDH, 1 mM nicotinamide adenine dinucleotide (NADH), 50 μ M PLP, and 0.25 μ M WT-Rv0812 or mutants. The buffer was premixed and incubated for 30 min. The assay was initiated by adding 25 μ l D-Ala for final concentrations ranging from 31 μ M to 32 mM. Enzyme activity was monitored by the decrease in absorbance at 340 nm, representing NADH consumption, using a Varioskan LUX multimode microplate reader (Thermo Fisher Scientific).

Kinetic measurements of Rv0812's ADCL activity were likewise obtained by using an LDH-coupled assay. ADCL activity assays were performed at 25°C in 100 mM Tris (pH 8.5) containing 5 mM MgCl₂, 100 mM (NH₄)₂SO₄, 5 U/ml LDH, 500 μ M NADH, 25 μ M PLP, 11 μ M EcPabB, and chorismate at concentrations ranging from 0 to 2 mM. The buffer was premixed and incubated for 30 min. The assay was initiated by adding 0.5 μ M WT-Rv0812 or mutants. PABA production was monitored using a Varioskan LUX multimode microplate reader (Thermo Fisher Scientific) at 340 nm to monitor the decrease in NADH concentration. For quantitative analysis of pyruvate production, only the 2 mM chorismate group was used.

For in vitro DAAT and ADCL kinetics assays, experiments were performed in triplicate for each protein construct and reported as average \pm SEM. Kinetic data were fitted with the Michaelis-Menten equation (Michaelis et al., 2011) using the JMP Pro 13 Software (SAS Institute).

Substrate competition assays

Substrate competition assays were conducted as described above in the presence or absence of varying concentrations of substrates. ADCL assays were conducted in the presence of EcPabB and 0.4 mM or 1.6 mM chorismate as a surrogate for the ADC substrate in the presence or absence of D-Ala (0, 7.5, or 30 mM) or D-Glu (0, 0.25, or 1 mM) as competing substrate. DAAT assays were conducted in the presence of D-Ala (7.5 or 30 mM) or D-Glu (0.25, or 1 mM) in the presence or absence of EcPabB and chorismate (0, 0.4, or 1.6 mM) as competing substrate. Kinetic

parameters in the presence or absence of competing substrate were determined by plotting the inverse velocity against the inverse substrate concentration on double reciprocal plots and calculating the inverse of the x- and y-intercepts.

Phylogenetic analysis

BLAST searches using the Rv0812 amino acid sequence were conducted against various bacterial phyla and classes with a maximum output of 100 hits for each group. BLAST hits were screened to include only those sequences with conservation of Arg26 as potentially Rv0812 like. Sequences were aligned with representative members of each type IV PLPDE subfamily using Clustal W2 and were subsequently placed into a phylogenetic tree using the neighbor joining method with BLOSUM62 to predict functional annotations. Phylogenetic trees were visualized using the interactive tree of life program (Letunic and Bork, 2019).

In vivo metabolomic profiling of *Mtb* strains

In vivo metabolic profiling of *Mtb* strains was conducted as previously described (Eoh and Rhee, 2013). A 1-ml culture (OD_{580 nm} = 1.0) of each strain was collected on a nitrocellulose filter and grown on 7H10 plates for 5 d at 37°C. Filters were subsequently transferred to swimming pools containing ~3 ml of Sauton's medium in the presence or absence of PABA (1 μ g/ml), DCS, PAS, WR99210, D-Ala, and/or D-Glu. Filters were collected following 24 h of exposure, and metabolic activity was quenched by placing cells in 1 ml of an ACN:methanol:H₂O (40:40:20) solution. Cells were lysed by mechanical disruption with 0.1-mm Zirconia beads (BioSpec Products) in a Precellys tissue homogenizer (cooled to 4°C) for 3 min at 6,500 rpm three times. Centrifugation enabled the separation of soluble cellular metabolites, which were then filtered through Spin-X (0.22 μ M) columns for removal from the BSL3 facility. Metabolite extracts were diluted 1:1 in LC-MS solvent B, centrifuged for 10 min at 10,000 \times g, and supernatant (2 μ l) was injected onto a Diamond Hydride column for LC-MS analysis as described above. For normalization of ion abundance to cell biomass, the residual protein concentration in lysates was quantified (BCA Protein Assay Kit; Thermo Fisher Scientific).

Drug susceptibility assays

Mtb cultures grown to mid-log phase in Sauton's medium were diluted in fresh medium to a starting OD_{580 nm} of 0.01. Varying concentrations of compounds in DMSO were added at 1% of the total volume. Following 6 d of exposure to compounds, cultures were serially diluted with 1 \times PBS containing 0.04% tyloxapol. Serial dilutions were streaked on 7H10 plates and allowed to recover for 21 d, at which point colonies were counted at appropriate dilutions.

Protein crystallization

Rv0812 was first crystallized without incubation with cofactor or compounds. Crystallization conditions (formulated by Hampton Research) were screened using a Mosquito liquid dispenser (TTP Labtech) using the sitting drop vapor diffusion technique in the Crystal Mation Intelli-Plate 96-3 low-profile

crystallization plate (Hampton Research). For each condition, 0.4 μ l protein (5 mg/ml) and 0.4 μ l crystallization formulation were mixed, and the mixture was equilibrated with 50 μ l crystallization solution in the reservoir well. Full-length WT Rv0812 protein crystals were further optimized via hanging drop vapor diffusion by incubating 2 μ l purified protein solution (5 mg/ml) with 1 μ l crystallization solution (1 M sodium citrate and 0.1 M sodium cacodylate [pH 7.1]) at 18°C for 3 d. Crystals formed as clusters during the first few optimizations. The microseeding method was applied to acquire larger and well-separated single crystals (Luft and DeTitta, 1999). A crystal cluster was taken from the optimized condition along with 10 μ l mother liquor. The cluster was then crushed by vortexing for 3 min with a Seed Bead kit (Hampton research). The mixture was added to 90 μ l mother liquor to prepare the 1:10 seed stock, which was further diluted to make 1:100 and 1:1,000 seed stocks. New crystals were obtained via hanging drop vapor diffusion by incubating 2 μ l purified protein solution (3 mg/ml) with 1 μ l seed stocks. The mixture was equilibrated with optimized crystallization conditions (1 M sodium citrate and 0.1 M sodium cacodylate [pH 7.1]) at 18°C for 3 d. The best crystals appeared in 1:1,000 dilution seed stock. These crystals were cryo-protected with 23% ethylene glycol and flash frozen before data collection. For PLP complex crystals, 0.2 mM PLP (pH adjusted to 6.6) was cocrystallized with 3 mg/ml Rv0812 using the above procedure. For PMP and AKG-bound crystals, 1 mM D-Glu and 0.2 mM PLP (pH adjusted to 6.6) were cocrystallized with 3 mg/ml Rv0812 using the same method as for PLP-bound crystals.

Data collection and structure determination

Data were collected at Argonne National Laboratory using the Advanced Photon Source beamlines 19ID and 23ID-D. All data were processed and reduced using HKL2000 (Otwinowski and Minor, 1997). The structure of apo-Rv0812 was solved by molecular replacement using MOLREP (Vagin and Teplyakov, 2010) in CCP4 (Winn et al., 2011) using the coordinates for the fold IV-transaminase (CpuTAI) from *Curtobacterium pusillum* from the PDB (accession no. 5K3W; Pavkov-Keller et al., 2016). The PLP-bound and PMP and AKG-bound structures were solved by molecular replacement using MOLREP in CCP4 with the solved apo-Rv0812 structure. Refinement and manual model building were performed with PHENIX (Adams et al., 2010) and COOT (Emsley and Cowtan, 2004), respectively.

Molecular docking

The simplified molecular-input line-entry system (SMILES) string of ADC was created by the JSME Structure Editor (Bienfait and Ertl, 2013) and the coordinates were generated through the CADD Group SMILES Translator (Sitzmann et al., 2008). ADC was placed into the active site of the PMP-containing Rv0812 structure—AKG, waters, and other ligands were removed from the model before docking—in COOT (Emsley and Cowtan, 2004). ADC was incorporated into the location according to the bound PMP. The active site docking model with the lowest global energy minimum was generated by the MolSoft ICM Chemist Pro Docking Program (Orry and Abagyan, 2012).

A model of the *A. thaliana* ADCL/DAAT was generated from the amino acid sequence of the enzyme using the Phyre2

webserver (Kelley et al., 2015). Structural superposition of Rv0812 with *A. thaliana* ADCL/DAAT was performed using Chimera (Pettersen et al., 2004).

Macromolecular assembly analysis

After acquiring Rv0812 structures, both apo- and PLP-bound structure coordinate files were uploaded to the program PDBe-PISA (Krissinel and Henrick, 2007) to analyze the macromolecular assemblies. Interactions across the interfaces were found. The buried surface area of the interfaces and the free energy of assembly dissociation (ΔG^{diss}) were calculated for both structures.

Data and software availability

The Apo, PLP-bound, and PMP and AKG-bound structures were deposited in the PDB (Berman et al., 2000) with accession nos. 6Q1Q, 6Q1R, and 6Q1S, respectively.

Online supplemental material

Fig. S1 provides additional evidence for the ability of Rv0812 to serve as both a DAAT and ADCL in the form of kinetic, structural, and phenotypic analysis. Bioinformatic analysis and structural homology modeling shown in Fig. S2 suggest that Rv0812 and similar sequences constitute a novel subgroup of type IV PLPDEs that are defined by their proposed ADCL/DAAT bifunctionality. Fig. S3 provides additional evidence for the ability of Rv0812 to serve as an ADCL and DAAT in vivo. Table S1 lists detailed parameters of the crystallography data and refinement statistic.

Acknowledgments

The authors thank Carl F. Nathan and Sumit Chakraborty for critical input and discussions.

This work was supported by the Bill and Melinda Gates Foundation TB Drug Accelerator (grant OPP1177930) and the National Institute of Allergy and Infectious Diseases (grants AI107774 and AI111143).

Author contributions: K.Y. Rhee, J.C. Sacchettini, and S. Ehrh designed the study; K.A. Black, L. Duan, L. Mandyoli, B.P. Selbach, and W. Xu performed experiments and analyzed the data; L. Duan and L. Mandyoli performed the structural studies; and K.A. Black, L. Duan, K.Y. Rhee, and J.C. Sacchettini wrote the manuscript with input from B.P. Selbach, W. Xu, and S. Ehrh.

Disclosures: The authors declare no competing interests exist.

Submitted: 14 October 2019

Revised: 16 February 2021

Accepted: 30 March 2021

References

- Adams, P.D., P.V. Afonine, G. Bunkóczi, V.B. Chen, I.W. Davis, N. Echols, J.J. Headd, L.W. Hung, G.J. Kapral, R.W. Grosse-Kunstleve, et al. 2010. PHENIX: a comprehensive Python-based system for macromolecular structure solution. *Acta Crystallogr. D Biol. Crystallogr.* 66:213–221. <https://doi.org/10.1107/S0907444909052925>
- Basset, G.J.C., S. Ravel, E.P. Quinlivan, R. White, J.J. Giavanonni, F. Rebeille, B.P. Nichols, K. Shinozaki, M. Seki, J.F. Gregory, et al. 2004. Folate

- synthesis in plants: the last step of the p-aminobenzoate branch is catalyzed by a plastidial aminodeoxychorismate lyase. *Plant J.* 40(4): 453–461. <https://doi.org/10.1111/j.1365-313X.2004.02231.x>
- Berman, H.M., J. Westbrook, Z. Feng, G. Gilliland, T.N. Bhat, H. Weissig, I.N. Shindyalov, and P.E. Bourne. 2000. The Protein Data Bank. *Nucleic Acids Res.* 28:235–242. <https://doi.org/10.1093/nar/28.1.235>
- Bhatia, M.B., S. Futaki, H. Ueno, J.M. Manning, D. Ringe, T. Yoshimura, and K. Soda. 1993. Kinetic and stereochemical comparison of wild-type and active-site K145Q mutant enzyme of bacterial D-amino acid transaminase. *J. Biol. Chem.* 268:6932–6938. [https://doi.org/10.1016/S0021-9258\(18\)53129-X](https://doi.org/10.1016/S0021-9258(18)53129-X)
- Bienfait, B., and P. Ertl. 2013. JSME: a free molecule editor in JavaScript. *J. Cheminform.* 5:24. <https://doi.org/10.1186/1758-2946-5-24>
- Chakraborty, S., T. Gruber, C.E. Barry III, H.I. Boshoff, and K.Y. Rhee. 2013. Para-aminosalicylic acid acts as an alternative substrate of folate metabolism in *Mycobacterium tuberculosis*. *Science*. 339:88–91. <https://doi.org/10.1126/science.1228980>
- Chim, N., J.E. Habel, J.M. Johnston, I. Krieger, L. Miallau, R. Sankaranarayanan, R.P. Morse, J. Bruning, S. Swanson, H. Kim, et al. 2011. The TB Structural Genomics Consortium: a decade of progress. *Tuberculosis (Edinb.)*. 91:155–172. <https://doi.org/10.1016/j.tube.2010.11.009>
- Christen, P., and P.K. Mehta. 2001. From cofactor to enzymes. The molecular evolution of pyridoxal-5'-phosphate-dependent enzymes. *Chem. Rev.* 1: 436–447. <https://doi.org/10.1002/tcr.10005>
- Cole, S.T., R. Brosch, J. Parkhill, T. Garnier, C. Churcher, D. Harris, S.V. Gordon, K. Eiglmeier, S. Gas, C.E. Barry III, et al. 1998. Deciphering the biology of *Mycobacterium tuberculosis* from the complete genome sequence. *Nature*. 393:537–544. <https://doi.org/10.1038/31159>
- David, S. 2001. Synergic activity of D-cycloserine and beta-chloro-D-alanine against *Mycobacterium tuberculosis*. *J. Antimicrob. Chemother.* 47: 203–206. <https://doi.org/10.1093/jac/47.2.203>
- de Carvalho, L.P., H. Zhao, C.E. Dickinson, N.M. Arango, C.D. Lima, S.M. Fischer, O. Ouerfelli, C. Nathan, and K.Y. Rhee. 2010. Activity-based metabolomic profiling of enzymatic function: identification of Rv1248c as a mycobacterial 2-hydroxy-3-oxoadipate synthase. *Chem. Biol.* 17: 323–332. <https://doi.org/10.1016/j.chembiol.2010.03.009>
- de Chiara, C., M. Homšak, G.A. Prosser, H.L. Douglas, A. Garza-Garcia, G. Kelly, A.G. Purkiss, E.W. Tate, and L.P.S. de Carvalho. 2020. D-Cycloserine destruction by alanine racemase and the limit of irreversible inhibition. *Nat. Chem. Biol.* 16:686–694. <https://doi.org/10.1038/s41589-020-0498-9>
- DeJesus, M.A., and T.R. Ioerger. 2013. A Hidden Markov Model for identifying essential and growth-defect regions in bacterial genomes from transposon insertion sequencing data. *BMC Bioinformatics*. 14:303. <https://doi.org/10.1186/1471-2105-14-303>
- DeJesus, M.A., E.R. Gerrick, W. Xu, S.W. Park, J.E. Long, C.C. Boutte, E.J. Rubin, D. Schnappinger, S. Ehrt, S.M. Fortune, et al. 2017a. Comprehensive Essentiality Analysis of the *Mycobacterium tuberculosis* Genome via Saturating Transposon Mutagenesis. *MBio*. 8:e02133-16. <https://doi.org/10.1128/mBio.02133-16>
- DeJesus, M.A., S. Nambi, C.M. Smith, R.E. Baker, C.M. Sasseti, and T.R. Ioerger. 2017b. Statistical analysis of genetic interactions in Tn-Seq data. *Nucleic Acids Res.* 45:e93. <https://doi.org/10.1093/nar/gkx128>
- Dubnau, E., J. Chan, V.P. Mohan, and I. Smith. 2005. Responses of mycobacterium tuberculosis to growth in the mouse lung. *Infect. Immun.* 73: 3754–3757. <https://doi.org/10.1128/IAI.73.6.3754-3757.2005>
- Ehrt, S., D. Schnappinger, and K.Y. Rhee. 2018. Metabolic principles of persistence and pathogenicity in *Mycobacterium tuberculosis*. *Nat. Rev. Microbiol.* 16:496–507. <https://doi.org/10.1038/s41579-018-0013-4>
- Emsley, P., and K. Cowtan. 2004. Coot: model-building tools for molecular graphics. *Acta Crystallogr. D Biol. Crystallogr.* 60:2126–2132. <https://doi.org/10.1107/S0907444904019158>
- Eoh, H., and K.Y. Rhee. 2013. Multifunctional essentiality of succinate metabolism in adaptation to hypoxia in *Mycobacterium tuberculosis*. *Proc. Natl. Acad. Sci. USA*. 110:6554–6559. <https://doi.org/10.1073/pnas.1219375110>
- Eschenfeldt, W.H., S. Lucy, C.S. Millard, A. Joachimiak, and I.D. Mark. 2009. A family of LIC vectors for high-throughput cloning and purification of proteins. *Methods Mol. Biol.* 498:105–115. https://doi.org/10.1007/978-1-59745-196-3_7
- Funakoshi, M., M. Sekine, M. Katane, T. Furuchi, M. Yohda, T. Yoshikawa, and H. Homma. 2008. Cloning and functional characterization of Arabidopsis thaliana D-amino acid aminotransferase--D-aspartate behavior during germination. *FEBS Journal*. 275(6):1188–1200. <https://doi.org/10.1111/j.1742-4658.2008.06279.x>
- Gautam, A., R. Vyas, and R. Tewari. 2011. Peptidoglycan biosynthesis machinery: a rich source of drug targets. *Crit. Rev. Biotechnol.* 31:295–336. <https://doi.org/10.3109/07388551.2010.525498>
- Gee, C.L., K.G. Papavinasundaram, S.R. Blair, C.E. Baer, A.M. Falick, D.S. King, J.E. Griffin, H. Venghatakrishnan, A. Zukauskas, J.R. Wei, et al. 2012. A phosphorylated pseudokinase complex controls cell wall synthesis in mycobacteria. *Sci. Signal.* 5:ra7. <https://doi.org/10.1126/scisignal.2002525>
- Green, J.M., and R.G. Matthews. 2007. Folate Biosynthesis, Reduction, and Polyglutamylation and the Interconversion of Folate Derivatives. *Ecosal Plus*. 2:1. <https://doi.org/10.1128/ecosalplus.3.6.3.6>
- Griffin, J.E., J.D. Gawronski, M.A. DeJesus, T.R. Ioerger, B.J. Akerley, and C.M. Sasseti. 2011. High-resolution phenotypic profiling defines genes essential for mycobacterial growth and cholesterol catabolism. *PLoS Pathog.* 7:e1002251. <https://doi.org/10.1371/journal.ppat.1002251>
- Hanson, A.D., A. Pribat, J.C. Waller, and V. de Crécy-Lagard. 2009. 'Unknown' proteins and 'orphan' enzymes: the missing half of the engineering parts list--and how to find it. *Biochem. J.* 425:1–11. <https://doi.org/10.1042/BJ20091328>
- Jhee, K.H., T. Yoshimura, E.W. Miles, S. Takeda, I. Miyahara, K. Hirotsu, K. Soda, Y. Kawata, and N. Esaki. 2000. Stereochemistry of the transamination reaction catalyzed by aminodeoxychorismate lyase from *Escherichia coli*: close relationship between fold type and stereochemistry. *J. Biochem.* 128:679–686. <https://doi.org/10.1093/oxfordjournals.jbchem.a022801>
- Kapopoulou, A., J.M. Lew, and S.T. Cole. 2011. The MycoBrowser portal: a comprehensive and manually annotated resource for mycobacterial genomes. *Tuberculosis (Edinb.)*. 91:8–13. <https://doi.org/10.1016/j.tube.2010.09.006>
- Kelley, L.A., S. Mezulis, C.M. Yates, M.N. Wass, and M.J. Sternberg. 2015. The Phyre2 web portal for protein modeling, prediction and analysis. *Nat. Protoc.* 10:845–858. <https://doi.org/10.1038/nprot.2015.053>
- Kieser, K.J., C. Baranowski, M.C. Chao, J.E. Long, C.M. Sasseti, M.K. Waldor, J.C. Sacchettini, T.R. Ioerger, and E.J. Rubin. 2015. Peptidoglycan synthesis in *Mycobacterium tuberculosis* is organized into networks with varying drug susceptibility. *Proc. Natl. Acad. Sci. USA*. 112:13087–13092. <https://doi.org/10.1073/pnas.1514135112>
- Krissinel, E., and K. Henrick. 2007. Inference of macromolecular assemblies from crystalline state. *J. Mol. Biol.* 372:774–797. <https://doi.org/10.1016/j.jmb.2007.05.022>
- Lechartier, B., J. Rybníček, A. Zumla, and S.T. Cole. 2014. Tuberculosis drug discovery in the post-post-genomic era. *EMBO Mol. Med.* 6:158–168. <https://doi.org/10.1002/emmm.201201772>
- Letunic, I., and P. Bork. 2019. Interactive Tree Of Life (iTOL) v4: recent updates and new developments. *Nucleic Acids Res.* 47(W1):W256–W259. <https://doi.org/10.1093/nar/gkz239>
- Lew, J.M., A. Kapopoulou, L.M. Jones, and S.T. Cole. 2011. TubercuList--10 years after. *Tuberculosis (Edinb.)*. 91:1–7. <https://doi.org/10.1016/j.tube.2010.09.008>
- Luft, J.R., and G.T. DeTitta. 1999. A method to produce microseed stock for use in the crystallization of biological macromolecules. *Acta Crystallogr. D Biol. Crystallogr.* 55:988–993. <https://doi.org/10.1107/S0907444999002085>
- Magnani, G., M. Lomazzi, and A. Peracchi. 2013. Completing the folate biosynthesis pathway in *Plasmodium falciparum*: p-aminobenzoate is produced by a highly divergent promiscuous aminodeoxychorismate lyase. *Biochem. J.* 455:149–155. <https://doi.org/10.1042/BJ20130896>
- Manning, J.M., N.E. Merrifield, W.M. Jones, and E.C. Gotschlich. 1974. Inhibition of bacterial growth by β -chloro-D-alanine. *Proc. Natl. Acad. Sci. USA*. 71:417–421. <https://doi.org/10.1073/pnas.71.2.417>
- Marchler-Bauer, A., Y. Bo, L. Han, J. He, C.J. Lanczycki, S. Lu, F. Chitsaz, M.K. Derbyshire, R.C. Geer, N.R. Gonzales, et al. 2017. CDD/SPARCLE: functional classification of proteins via subfamily domain architectures. *Nucleic Acids Res.* 45(D1):D200–D203. <https://doi.org/10.1093/nar/gkw1129>
- Marshall, D.D., S. Halouska, D.K. Zinniel, R.J. Fenton, K. Kenealy, H.K. Chahal, G. Rathniah, R.G. Barletta, and R. Powers. 2017. Assessment of Metabolic Changes in *Mycobacterium smegmatis* Wild-Type and alr Mutant Strains: Evidence of a New Pathway of d-Alanine Biosynthesis. *J. Proteome Res.* 16:1270–1279. <https://doi.org/10.1021/acs.jproteome.6b00871>
- Martínez del Pozo, A., M. Merola, H. Ueno, J.M. Manning, K. Tanizawa, K. Nishimura, S. Asano, H. Tanaka, K. Soda, D. Ringe, et al. 1989a. Activity and spectroscopic properties of bacterial D-amino acid transaminase

- after multiple site-directed mutagenesis of a single tryptophan residue. *Biochemistry*. 28:510–516. <https://doi.org/10.1021/bi00428a015>
- Martínez del Pozo, A., M. Merola, H. Ueno, J.M. Manning, K. Tanizawa, K. Nishimura, K. Soda, and D. Ringe. 1989b. Stereospecificity of reactions catalyzed by bacterial D-amino acid transaminase. *J. Biol. Chem.* 264: 17784–17789. [https://doi.org/10.1016/S0021-9258\(19\)84641-0](https://doi.org/10.1016/S0021-9258(19)84641-0)
- Mehta, P.K., and P. Christen. 2000. The molecular evolution of pyridoxal-5'-phosphate-dependent enzymes. *Adv. Enzymol. Relat. Areas Mol. Biol.* 74: 129–184. <https://doi.org/10.1002/9780470123201.ch4>
- Michaelis, L., M.L. Menten, K.A. Johnson, and R.S. Goody. 2011. The original Michaelis constant: translation of the 1913 Michaelis-Menten paper. *Biochemistry*. 50:8264–8269. <https://doi.org/10.1021/bi201284u>
- Miles, E.W. 1985. Transamination as a side reaction of other phosphopyridoxal enzymes. In *Transaminases*. P. Christen and D.E. Metzler, editors. John Wiley & Sons, New York. 470–481.
- Mortuza, R., H.L. Aung, G. Taiarou, H.K. Opel-Reading, T. Kleffmann, G.M. Cook, and K.L. Krause. 2018. Overexpression of a newly identified d-amino acid transaminase in *Mycobacterium smegmatis* complements glutamate racemase deletion. *Mol. Microbiol.* 107:198–213. <https://doi.org/10.1111/mmi.13877>
- Nakai, T., H. Mizutani, I. Miyahara, K. Hirotsu, S. Takeda, K.-H. Jhee, T. Yoshimura, and N. Esaki. 2000. Three-dimensional structure of 4-amino-4-deoxychorismate lyase from *Escherichia coli*. *J. Biochem.* 128: 29–38. <https://doi.org/10.1093/oxfordjournals.jbchem.a022727>
- Nixon, M.R., K.W. Saionz, M.S. Koo, M.J. Szymonifka, H. Jung, J.P. Roberts, M. Nandakumar, A. Kumar, R. Liao, T. Rustad, et al. 2014. Folate pathway disruption leads to critical disruption of methionine derivatives in *Mycobacterium tuberculosis*. *Chem. Biol.* 21:819–830. <https://doi.org/10.1016/j.chembiol.2014.04.009>
- O'Rourke, P.E., T.C. Eadsforth, P.K. Fyfe, S.M. Shepherd, and W.N. Hunter. 2011. *Pseudomonas aeruginosa* 4-amino-4-deoxychorismate lyase: spatial conservation of an active site tyrosine and classification of two types of enzyme. *PLoS One*. 6:e24158. <https://doi.org/10.1371/journal.pone.0024158>
- Orry, A.J., and R. Abagyan. 2012. Preparation and refinement of model protein-ligand complexes. *Methods Mol. Biol.* 857:351–373. https://doi.org/10.1007/978-1-61779-588-6_16
- Otwinowski, Z., and W. Minor. 1997. Processing of X-ray diffraction data collected in oscillation mode. *Methods Enzymol.* 276:307–326. [https://doi.org/10.1016/S0076-6879\(97\)76066-X](https://doi.org/10.1016/S0076-6879(97)76066-X)
- Padmanabhan, B., Y. Bessho, A. Ebihara, S.V. Antonyuk, M.J. Ellis, R.W. Strange, S. Kuramitsu, N. Watanabe, S.S. Hasnain, and S. Yokoyama. 2009. Structure of putative 4-amino-4-deoxychorismate lyase from *Thermus thermophilus* HB8. *Acta Crystallogr. Sect. F Struct. Biol. Cryst. Commun.* 65:1234–1239. <https://doi.org/10.1107/S1744309109050052>
- Parsons, J.F., P.Y. Jensen, A.S. Pachikara, A.J. Howard, E. Eisenstein, and J.E. Ladner. 2002. Structure of *Escherichia coli* aminodeoxychorismate synthase: architectural conservation and diversity in chorismate-utilizing enzymes. *Biochemistry*. 41:2198–2208. <https://doi.org/10.1021/bi015791b>
- Pavkov-Keller, T., G.A. Strohmeier, M. Diepold, W. Peeters, N. Smeets, M. Schürmann, K. Gruber, H. Schwab, and K. Steiner. 2016. Discovery and structural characterisation of new fold type IV-transaminases exemplify the diversity of this enzyme fold. *Sci. Rep.* 6:38183. <https://doi.org/10.1038/srep38183>
- Peisach, D., D.M. Chipman, P.W. Van Ophem, J.M. Manning, and D. Ringe. 1998. Crystallographic study of steps along the reaction pathway of D-amino acid aminotransferase. *Biochemistry*. 37:4958–4967. <https://doi.org/10.1021/bi972884d>
- Percudani, R., and A. Peracchi. 2009. The B6 database: a tool for the description and classification of vitamin B6-dependent enzymatic activities and of the corresponding protein families. *BMC Bioinformatics*. 10: 273. <https://doi.org/10.1186/1471-2105-10-273>
- Pettersen, E.F., T.D. Goddard, C.C. Huang, G.S. Couch, D.M. Greenblatt, E.C. Meng, and T.E. Ferrin. 2004. UCSF Chimera—a visualization system for exploratory research and analysis. *J. Comput. Chem.* 25:1605–1612. <https://doi.org/10.1002/jcc.20084>
- Prosser, G.A., and L.P. de Carvalho. 2013a. Metabolomics Reveal d-Alanine:d-Alanine Ligase As the Target of d-Cycloserine in *Mycobacterium tuberculosis*. *ACS Med. Chem. Lett.* 4:1233–1237. <https://doi.org/10.1021/ml400349n>
- Prosser, G.A., and L.P. de Carvalho. 2013b. Reinterpreting the mechanism of inhibition of *Mycobacterium tuberculosis* D-alanine:D-alanine ligase by D-cycloserine. *Biochemistry*. 52:7145–7149. <https://doi.org/10.1021/bi400839f>
- Prosser, G.A., and L.P.S. de Carvalho. 2013c. Kinetic mechanism and inhibition of *Mycobacterium tuberculosis* D-alanine:D-alanine ligase by the antibiotic D-cycloserine. *FEBS J.* 280:1150–1166. <https://doi.org/10.1111/febs.12108>
- Prosser, G.A., A. Rodenburg, H. Khoury, C. de Chiara, S. Howell, A.P. Snijders, and L.P. de Carvalho. 2016. Glutamate Racemase Is the Primary Target of β -Chloro-d-Alanine in *Mycobacterium tuberculosis*. *Antimicrob. Agents Chemother.* 60:6091–6099. <https://doi.org/10.1128/AAC.01249-16>
- Pruitt, K.D., T. Tatusova, and D.R. Maglott. 2007. NCBI reference sequences (RefSeq): a curated non-redundant sequence database of genomes, transcripts and proteins. *Nucleic Acids Res.* 35(Database):D61–D65. <https://doi.org/10.1093/nar/gkl842>
- Saghatelian, A., and B.F. Cravatt. 2005. Assignment of protein function in the postgenomic era. *Nat. Chem. Biol.* 1:130–142. <https://doi.org/10.1038/nchembio0805-130>
- Sitzmann, M., I.V. Filippov, and M.C. Nicklaus. 2008. Internet resources integrating many small-molecule databases. *SAR QSAR Environ. Res.* 19: 1–9. <https://doi.org/10.1080/10629360701843540>
- Smith, I. 2003. *Mycobacterium tuberculosis* pathogenesis and molecular determinants of virulence. *Clin. Microbiol. Rev.* 16:463–496. <https://doi.org/10.1128/CMR.16.3.463-496.2003>
- Sugio, S., G.A. Petsko, J.M. Manning, K. Soda, and D. Ringe. 1995. Crystal structure of a D-amino acid aminotransferase: how the protein controls stereoselectivity. *Biochemistry*. 34:9661–9669. <https://doi.org/10.1021/bi00030a002>
- Thiede, J.M., S.L. Kordus, B.J. Turman, J.A. Buonomo, C.C. Aldrich, Y. Minato, and A.D. Baughn. 2016. Targeting intracellular p-aminobenzoic acid production potentiates the anti-tubercular action of antifolates. *Sci. Rep.* 6:38083. <https://doi.org/10.1038/srep38083>
- Vagin, A., and A. Teplyakov. 2010. Molecular replacement with MOLREP. *Acta Crystallogr. D Biol. Crystallogr.* 66:22–25. <https://doi.org/10.1107/S0907444909042589>
- Waterhouse, A.M., J.B. Procter, D.M.A. Martin, M. Clamp, and G.J. Barton. 2009. Jalview Version 2—a multiple sequence alignment editor and analysis workbench. *Bioinformatics*. 25:1189–1191. <https://doi.org/10.1093/bioinformatics/btp033>
- Wattam, A.R., D. Abraham, O. Dalay, T.L. Disz, T. Driscoll, J.L. Gabbard, J.J. Gillespie, R. Gough, D. Hix, R. Kenyon, et al. 2014. PATRIC, the bacterial bioinformatics database and analysis resource. *Nucleic Acids Res.* 42(D1): D581–D591. <https://doi.org/10.1093/nar/gkt1099>
- Winn, M.D., C.C. Ballard, K.D. Cowtan, E.J. Dodson, P. Emsley, P.R. Evans, R.M. Keegan, E.B. Krissinel, A.G. Leslie, A. McCoy, et al. 2011. Overview of the CCP4 suite and current developments. *Acta Crystallogr. D Biol. Crystallogr.* 67:235–242. <https://doi.org/10.1107/S0907444910045749>
- World Health Organization. 2020. Global Tuberculosis Report. <https://apps.who.int/iris/bitstream/handle/10665/336069/9789240013131-eng.pdf> (accessed 04/22/2021)
- Xu, W., M.A. DeJesus, N. Rücker, C.A. Engelhart, M.G. Wright, C. Healy, K. Lin, R. Wang, S.W. Park, T.R. Ioerger, et al. 2017. Chemical Genetic Interaction Profiling Reveals Determinants of Intrinsic Antibiotic Resistance in *Mycobacterium tuberculosis*. *Antimicrob. Agents Chemother.* 61:e01334–17. <https://doi.org/10.1128/AAC.01334-17>
- Ye, Q.Z., J. Liu, and C.T. Walsh. 1990. p-Aminobenzoate synthesis in *Escherichia coli*: purification and characterization of PabB as aminodeoxychorismate synthase and enzyme X as aminodeoxychorismate lyase. *Proc. Natl. Acad. Sci. USA*. 87:9391–9395. <https://doi.org/10.1073/pnas.87.23.9391>
- Yoshimura, T., K. Nishimura, J. Ito, N. Esakik, H. Kagamiyama, J.M. Manning, and K. Soda. 1993. Unique stereospecificity of D-amino acid aminotransferase and branched-chain L-amino acid aminotransferase for C-4' hydrogen transfer of the coenzyme. *J. Am. Chem. Soc.* 115:3897–3900. <https://doi.org/10.1021/ja00063a007>
- Zhang, Y., L. Bai, and Z. Deng. 2009. Functional characterization of the first two actinomycete 4-amino-4-deoxychorismate lyase genes. *Microbiology (Reading)*. 155:2450–2459. <https://doi.org/10.1099/mic.0.026336-0>
- Zhang, Y.J., T.R. Ioerger, C. Huttenhower, J.E. Long, C.M. Sassetti, J.C. Sacchettini, and E.J. Rubin. 2012. Global assessment of genomic regions required for growth in *Mycobacterium tuberculosis*. *PLoS Pathog.* 8: e1002946. <https://doi.org/10.1371/journal.ppat.1002946>

Supplemental material

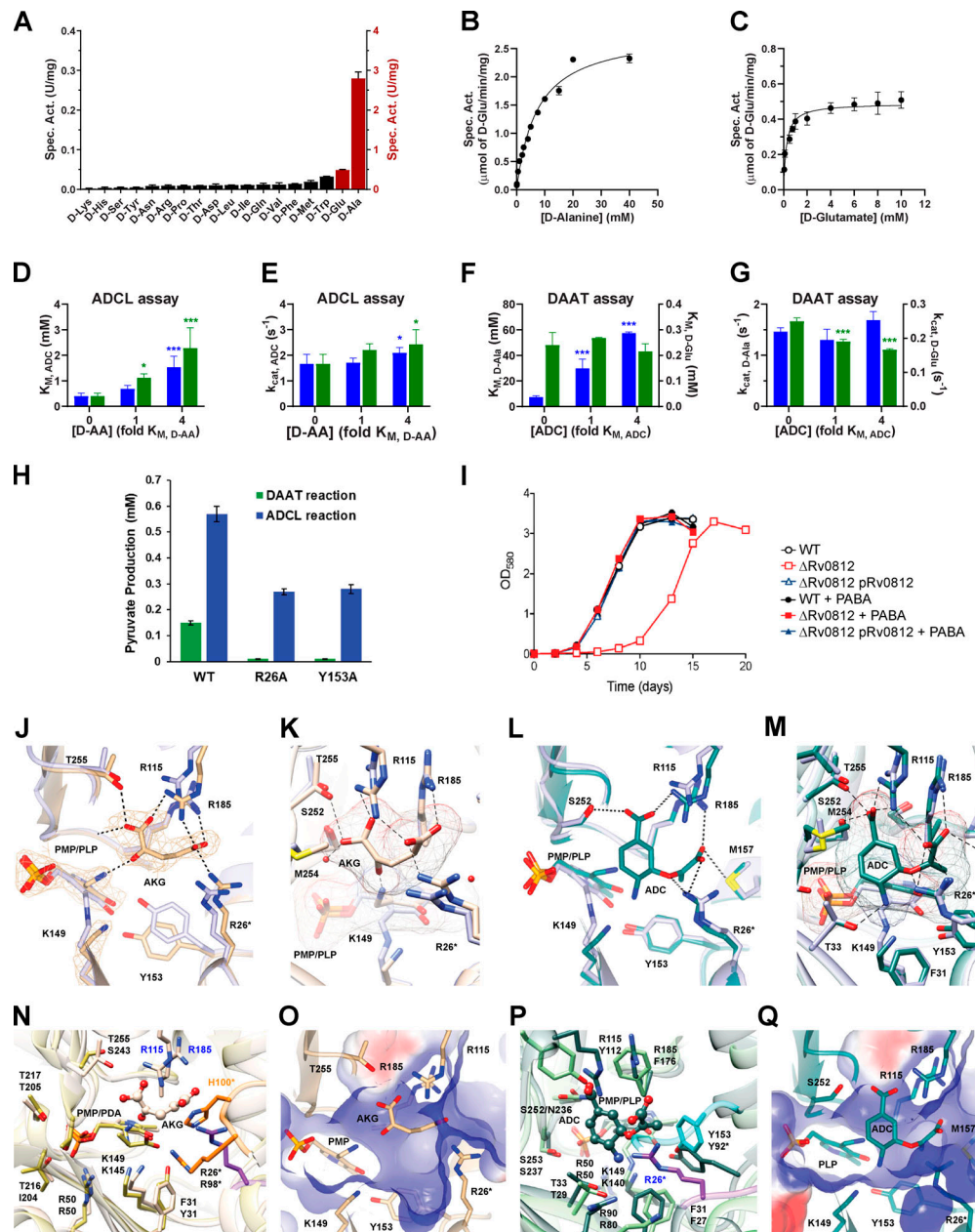


Figure S1. Structural, kinetic, and phenotypic analysis demonstrate the ability of Rv0812 to serve as both a DAAT and ADCL. (A) Rv0812 DAAT activity is restricted to D-Ala and D-Glu. Reaction aliquots containing 0.5 μ M Rv0812, 50 μ M PLP, 10 mM AKG, and 1 mM of each D-amino acid were quenched at various time points for LC-MS analysis. Activity was quantified by assessing substrate depletion over time and normalizing to a standard curve. Specific activities with D-Ala and D-Glu are plotted on the right y-axis, and specific activity (spec. act.) with other substrates is plotted on the left y-axis. (B and C) Activity profile of Rv0812 DAAT reactions. The rate of pyruvate formation (B) or D-Glu consumption (C) was determined in reactions with 0.25 μ M Rv0812, 5 mM AKG or pyruvate, 50 μ M PLP, and varied substrate concentrations at pH 8.5. Data were fitted to the Michaelis-Menten equation to give kinetic parameters: (A) $V_{\max} = 2.8 \pm 0.16$ U/mg and $K_M = 7.3 \pm 1.06$ mM; and (B) $V_{\max} = 0.49 \pm 0.019$ U/mg and $K_M = 0.24 \pm 0.05$ mM. (D–G) Substrate competition assays demonstrated the impact of DAAT substrates on ADCL activity (D and E) and vice versa (F and G). The x-axis indicates the concentration of D-amino acid or chorismate relative to the K_M . The y-axis indicates the kinetic constants obtained in the presence or absence of competing substrate. Blue and green bars indicate the presence of D-Ala or D-Glu, respectively. Each column represents the mean \pm SD ($n = 6$; *, $P < 0.05$; ***, $P < 0.001$) compared with parameters in the absence of competing substrate. (H) Pyruvate produced in DAAT (green) and ADCL (blue) reactions. (I) Growth of WT *Mtb*, Δ Rv0812, and Δ Rv0812::Rv0812 in the presence or absence of PABA (1 μ g/ml). (J–Q) Active site of AKG-bound Rv0812 and ADC-docked model. (J–M) Superposition of PLP-bound Rv0812 (purple) with AKG-bound form (ivory; J and K), and with ADC-docked model (teal; L and M). The AKG molecule and waters were removed before docking ADC into the active site. The mesh surface of AKG, ADC, and PMP is shown. H-bonds formed with protein side chains are shown as dashed lines (J–M), and the |(2Fo)–(Fc)| electron density map, contoured at 1.2 σ , of PLP and AKG (J) is shown as chicken wire. Side chains of residues neighboring AKG and ADC (within 5 Å) are shown (K and M). (N and P) Superposition of PDA-containing BsDAAT (yellow) with AKG-bound Rv0812 (N), and superposition of PLP-containing PaADCL (green) with ADC-docked Rv0812 (coral; P). BsDAAT and PaADCL interdomain loops are shown in orange and cyan, respectively. The loop from Rv0812 containing Arg26* is shown in purple. Conserved residues forming the active site are labeled in the order of Rv0812/BsDAAT or Rv0812/PaADCL. (O and Q) Electrostatic surface of Rv0812 in AKG-bound form (O) and ADC-docked model (Q).

A

<i>D. hafniense</i> ADCL	25 DRGQA	GDAL	ETLRAHR	-- GELPWWDAHWARLSQ	-- GAGRLGLALPDPRVRSEADLLAQ	-- ADG	-----	VL	LILSRGAQGRG	APPAQAEVPTLSRHLPP	-- PAR	-----	AGGLRLRWCAALRLGEQ	138											
<i>P. aeruginosa</i> ADCL	17 DRGLA	GDGL	ETLAVRA	-- GTPRLRLERHARLEE	-- GCRLRAIFI	-- DAAALRQELLAFCAALGDD	-----	VAL	LIVTRGEGRLG	APPAEASPRRLSGSPRPA	-----	PERHWQGVRLFACRTRLAEG	133												
<i>S. oneidensis</i> ADCL	16 DRGLA	GDGL	ATMRSSK	-- KQILFFQHQARLET	-- GAARLGFQWMSPALAEQDLTAAQTPQH	-----	CI	LMVTRGVGGRG	APPEQVNVTEVSVNHP	IPAYAAWQGGQIRLTKSAVRLAEQ	-----	133													
<i>E. coli</i> ADCL	16 DRATO	GDGC	ETARVID	-- QKVLISAHQIRLQD	-- AGCLMISCDPFWGLQEMTKLAAEQNG	-----	VL	IVISRGSGGGRG	STLNSGPATRLISVTATPA	YDRLRNEGILITLSPVRLGRN	-----	133													
<i>V. cholerae</i> ADCL	16 DRSTG	GDGC	ETILTKE	-- GQGVGWSHAKRLQA	-- CLDILHPIEPFNWVRWGLQSMILPQSKA	-----	GL	IHIISRGLOGGRG	STQVSESIVTISAFATPA	YQAWDRGKLAVGICGRRMLN	-----	133													
<i>Streptomyces</i> ADCL-1	15 ASIAL	HYGH	ETTLVEN	-- GRVRGLDLHLERLR	-- DCRTLFDAAALDPRVRKLARRAAPTQGRAT	-----	-----	VVTVDPALNLG	IAADARPGILVTSRPAADK	PGPLRVRSVVRH	-----	123													
<i>Mtb</i> Rv0812	21 DLAAV	GDGV	ETLLVRD	-- GRACLVEAHQLRLTQ	-- SARLMDLPEDLPWRRAVEVATQWVAST	-----	ADG	EALILYSRGREGG	-- SAPATVVMVSPVPAV	IGARRDGVSAITLDRGLPADGGDAM	-----	141													
<i>A. bacterium</i> ADCL	25 DIOVL	GDGV	ETLLVRG	-- GRARTVEQHLRLVS	-- SAAAAGLPTDPRDDWRLAIDVAEQWDAER	-----	EGAL	LIVTRGREGG	-- SEPTALLTPVAERVYKARADGVSVTLERQVSVLASKA	143															
<i>C. difficile</i> ADCL	25 DLAAV	GDGI	ETLLVRA	-- GRPFVRVHLERLAR	-- SAAAMELGTFDQDWRGVETATGAWVEKHGS	-----	AGEAL	LIVTRGREGG	-- SAPATVTVDAVDRVAARAGVRRVTLDRGFIIDLASSA	147															
<i>Streptomyces</i> ADCL-2	21 DLGLL	GDGV	ETLLVRD	-- GRPFELRPHLERLAR	-- SAAMLDPEDPLAAWEAAQGVVDHNSGPA	-----	ETAL	LIVTRGIDDDPEAKPGFALOVE	IDEKVOARAVEGVAITLREGIEPLDRAEA	143															
<i>S. aureus</i> DAAT	35 ELSTG	GDGV	ESLGVVD	-- GHAEVVPHLERLAH	-- SARLCLDPVPNLAQWRQIDAHAQAAGL	-----	AGESV	LILSRGVEHG	-- PTFAMWTAAPAD	-- FSAVRERGVRRVTLDRGYLDGAAERA	155														
<i>C. pusillum</i> DAAT/RATA	46 DLGIT	GDGV	ETIAVID	-- GHQALELHLERLAH	-- SAALDLPEDPAAVWREAVLAQVADYRSRNGD	-----	GGEL	FALILTRGIEGE	-- GRPSGVWFVDEGED	-- FSQGR	-- LGIRVTVTLDRGYLDGAAERA	166													
<i>A. thaliani</i> ADCL/DAAT	27 DHMVH	GHGV	ETALILN	-- GTLYELDQHLRLIR	-- SASMAKILPFPDRETKIRLIGTVSVSGCR	-----	DGSL	YMLSAQPGDFLLSPSQCLKPTLYA	IVIKTNFINFIPGVKVTSSIPFIK	-----	142														
<i>Desulfotalea</i> AAT	22 DL SVI	GYGV	DFLRTYD	-- GVPFRLQEHLSRLKN	-- SARLIDILNLPFPLEKIEALILKGLSLSRMT	-----	EKNV	IITGGLSANGISPDGAPQLLMI	TATESFPASFQDGKVLITSHVNR	-----	137														
<i>N. cyanobacterium</i> AAT	24 DLGIV	GYGV	DYLRITYN	-- GIPFLQEHILQRLQK	-- SAEILGILNLPWSTQIEALIEQTLKRNKLP	-----	EANI	IVVTGGASDDFITPPEQPSLILV	SPVSGVQVVEYQGVKLITQMER	-----	139														
<i>S. negevensis</i> BCAT/AAT	23 DLSIM	GYGV	DFLRTYQ	-- KLPFLRWHLRFEA	-- SAKIEIPLSPMNEVDVIEQLLEKAPYP	-----	EANI	KIFLTGGQSTQVLPEDRPTFFALV	PPVPRIFPKMEYEGKGVLTIEYER	-----	138														
<i>G. endophyticus</i> AAT	21 DLALO	GYGI	DFFRVRN	-- KKPFLLEDHLRFEA	-- SAGKMLQSPVDNRLDTIILITVEKNLIS	-----	DAGV	VLLTGGYAEQDVT	-- ITQPNLIVVVOFPKYPSEQGLQSGVKIITVNER	-----	135														
<i>Bacillus</i> YM-1 DAAT	21 DRGYV	GDGV	EVVKVYN	-- GHMPYVNEHLRFLYA	-- SAEKIRLIVPTTKDVKFHLHLHELVEKNELN	-----	TGHI	FQVTRGT	-- SPK	-- QFFPENT	-- VKPVI	-- IGTAKENPRPLE	-- LNEKGVKATFVEDI	137											
<i>L. sphaericus</i> DAAT	22 DRGYV	GDGI	EVVKVYN	-- GHMPYVNEHLRFLYA	-- SAEKIRLIVPTTKDVKFHLHLHELVEKNELN	-----	TGHI	FQVTRGT	-- SPK	-- QFFPENT	-- VKPVI	-- IGTAKENPRPLE	-- LNEKGVKATFVEDI	137											
<i>L. monocytogenes</i> DAAT	22 DRGYV	GDGV	EVVKVYN	-- GHMPYVNEHLRFLYA	-- SAEKIRLIVPTTKDVKFHLHLHELVEKNELN	-----	TGHI	FQVTRGT	-- SPK	-- QFFPENT	-- VKPVI	-- IGTAKENPRPLE	-- LNEKGVKATFVEDI	137											
<i>L. pneumophila</i> DAAT	22 DRGFL	GDGV	EVVKVYN	-- GHMPYVNEHLRFLYA	-- SAEKIRLIVPTTKDVKFHLHLHELVEKNELN	-----	TGHI	FQVTRGT	-- SPK	-- QFFPENT	-- VKPVI	-- IGTAKENPRPLE	-- LNEKGVKATFVEDI	137											
<i>B. paraptusiss</i> DAAT	22 DRGFL	GDGV	EVVKVYN	-- GHMPYVNEHLRFLYA	-- SAEKIRLIVPTTKDVKFHLHLHELVEKNELN	-----	TGHI	FQVTRGT	-- SPK	-- QFFPENT	-- VKPVI	-- IGTAKENPRPLE	-- LNEKGVKATFVEDI	137											
<i>M. loti</i> DAAT	23 DRGYV	ADGV	EVVKVYN	-- GHMPYVNEHLRFLYA	-- SAEKIRLIVPTTKDVKFHLHLHELVEKNELN	-----	TGHI	FQVTRGT	-- SPK	-- QFFPENT	-- VKPVI	-- IGTAKENPRPLE	-- LNEKGVKATFVEDI	137											
<i>D. hafniense</i> ADCL	139 P	-----	ALAGLKHCH	-- LEQVLARAEWD	PDIDEGLLRNAAGEV	-----	ATAAN	FVLHA	-----	GQWTPPVDRGVAGI	CRQLRIE	SG	-----	ARVAALTADELGRADAI	FLCN	AVRG	240								
<i>P. aeruginosa</i> ADCL	134 P	-----	LALGKHLN	-- LEQVLARAEWD	DAGAEGLMLDVHVRV	-----	GVFS	NLLVL	-----	GTVLAPDRRCVAGV	VMRAELLERAEG	IGVP	-----	LAIRVMSALATADEV	FLCN	SQFQ	240								
<i>S. oneidensis</i> ADCL	134 P	-----	LALGKHLN	-- LEQVLARAEWD	DAGAEGLMLDVHVRV	-----	GVFS	NLLVL	-----	GTVLAPDRRCVAGV	VMRAELLERAEG	IGVP	-----	LAIRVMSALATADEV	FLCN	SQFQ	240								
<i>E. coli</i> ADCL	134 P	-----	LALGKHLN	-- LEQVLARAEWD	DAGAEGLMLDVHVRV	-----	GVFS	NLLVL	-----	GTVLAPDRRCVAGV	VMRAELLERAEG	IGVP	-----	LAIRVMSALATADEV	FLCN	SQFQ	240								
<i>V. cholerae</i> ADCL	134 P	-----	LALGKHLN	-- LEQVLARAEWD	DAGAEGLMLDVHVRV	-----	GVFS	NLLVL	-----	GTVLAPDRRCVAGV	VMRAELLERAEG	IGVP	-----	LAIRVMSALATADEV	FLCN	SQFQ	240								
<i>Streptomyces</i> ADCL-1	124 R	-----	DLPEVKS	SG	CPTLLRRGAQAGAGD	VFSTQDGVIL	-----	EGGT	WNVLVRD	-----	GEVVWPGVE	LAQTT	TRQLLRATDGP	-----	TELVGLADLDS	VEAFAT	AAVG	223							
<i>Mtb</i> Rv0812	142 PW	-----	LISAKTLS	AVNMAVLRHAARGAGD	VFSTQDGVIL	-----	OPRST	TVIATD	GGQGGGNFL	PTPPWYPI	LRGT	TQGA	LFVARAKGYD	-----	CDYRALRVAD	LDSSQ	IWLVS	SMTL	256						
<i>A. bacterium</i> ADCL	144 PW	-----	QLLGAKTLS	ATNMAALRHAESL	AGDGVIVISSEGFVL	-----	OPRST	SVLVARG	-----	RTLITPP	PEQGI	LPST	TQGA	LFVARAKGYD	-----	VRYEP	VRPADL	VADGVWLV	SVAL	251					
<i>C. difficile</i> ADCL	144 PW	-----	QLLGAKTLS	ATNMAALRHAESL	AGDGVIVISSEGFVL	-----	OPRST	SVLVARG	-----	RTLITPP	PEQGI	LPST	TQGA	LFVARAKGYD	-----	VRYEP	VRPADL	VADGVWLV	SVAL	251					
<i>Streptomyces</i> ADCL-2	144 PW	-----	QLLGAKTLS	ATNMAALRHAESL	AGDGVIVISSEGFVL	-----	OPRST	SVLVARG	-----	RTLITPP	PEQGI	LPST	TQGA	LFVARAKGYD	-----	VRYEP	VRPADL	VADGVWLV	SVAL	251					
<i>S. aureus</i> DAAT	156 PW	-----	QLLGAKTLS	AVNMAALRHAARGAGD	VFSTQDGVIL	-----	OPRST	TVIATD	GGQGGGNFL	PTPPWYPI	LRGT	TQGA	LFVARAKGYD	-----	CDYRALRVAD	LDSSQ	IWLVS	SMTL	256						
<i>C. pusillum</i> DAAT/RATA	167 PW	-----	LLAGAKTLS	ATNRAAGREARRAGD	VFSTQDGVIL	-----	OPRST	SVLVARG	-----	RTLITPP	PEQGI	LPST	TQGA	LFVARAKGYD	-----	VRYEP	VRPADL	VADGVWLV	SVAL	251					
<i>A. thaliani</i> ADCL/DAAT	143 PP	-----	EFATVKS	VN	LNPLVSGMEAEAKAGAT	AGIVWCKDGFIA	-----	OPN	MNVAVVN	-----	GGKEL	VMPFRD	NVL	SGCATKRLT	LAELQVLSGK	ILKTVKVM	DVTV	DEGDKADEMML	IGIP	256					
<i>Desulfotalea</i> AAT	139	-----	FLPAGKTLN	ISAILQGSQRANA	IDALVYVQGGVLE	-----	DTTNN	FFVRD	-----	GRIT	TPCD	RVLP	GI	TRGVVIL	LAQRT	ME	-----	LIERP	HNKE	IRL	FDV	ISVKE	241		
<i>N. cyanobacterium</i> AAT	140	-----	FLPAGKTLN	ISAILQGSQRANA	IDALVYVQGGVLE	-----	DTTNN	FFVRD	-----	GRIT	TPCD	RVLP	GI	TRGVVIL	LAQRT	ME	-----	LIERP	HNKE	IRL	FDV	ISVKE	241		
<i>S. negevensis</i> BCAT/AAT	139	-----	FLPAGKTLN	ISAILQGSQRANA	IDALVYVQGGVLE	-----	DTTNN	FFVRD	-----	GRIT	TPCD	RVLP	GI	TRGVVIL	LAQRT	ME	-----	LIERP	HNKE	IRL	FDV	ISVKE	241		
<i>G. endophyticus</i> AAT	135	-----	ELPDIKTIN	QKAIMTPAKVKAAN	AVDLYVH	HDGILISE	-----	PRCN	FFIVTG	-----	EDV	IKTPDQ	QILL	GVTRKKVIL	QLARKK	YK	-----	VEEC	IS	LDNDVYNAKE	FAFF	STKR	238		
<i>Bacillus</i> YM-1 DAAT	139 RW	-----	LRCDIKSLN	LGAVLAKGEAEHEKQ	YEAALHRRN	TVTE	-----	GSNN	SVFGIK	-----	DG	ILYTHP	ANNM	LKGI	TRDVI	IACANE	INMP	-----	VKE	IFPT	THEAL	KND	FDV	ITSE	244
<i>L. sphaericus</i> DAAT	139 RW	-----	LRCDIKSLN	LGAVLAKGEAEHEKQ	YEAALHRRN	TVTE	-----	GSNN	SVFGIK	-----	DG	ILYTHP	ANNM	LKGI	TRDVI	IACANE	INMP	-----	VKE	IFPT	THEAL	KND	FDV	ITSE	244
<i>L. monocytogenes</i> DAAT	149	-----	LRCDIKSLN	LGAVLAKGEAEHEKQ	YEAALHRRN	TVTE	-----	GSNN	SVFGIK	-----	DG	ILYTHP	ANNM	LKGI	TRDVI	IACANE	INMP	-----	VKE	IFPT	THEAL	KND	FDV	ITSE	244
<i>L. pneumophila</i> DAAT	139 RW	-----	LRCDIKSLN	LGAVLAKGEAEHEKQ	YEAALHRRN	TVTE	-----	GSNN	SVFGIK	-----	DG	ILYTHP	ANNM	LKGI	TRDVI	IACANE	INMP	-----	VKE	IFPT	THEAL	KND	FDV	ITSE	244
<i>B. paraptusiss</i> DAAT	141 RW	-----	LRCDIKSLN	LGAVLAKGEAEHEKQ	YEAALHRRN	TVTE	-----	GSNN	SVFGIK	-----	DG	ILYTHP	ANNM	LKGI	TRDVI	IACANE	INMP	-----	VKE	IFPT	THEAL	KND	FDV	ITSE	244
<i>M. loti</i> DAAT	142 RW	-----	LRCDIKSLN	LGAVLAKGEAEHEKQ	YEAALHRRN	TVTE	-----	GSNN	SVFGIK	-----	DG	ILYTHP	ANNM	LKGI	TRDVI	IACANE	INMP	-----	VKE	IFPT	THEAL	KND	FDV	ITSE	244

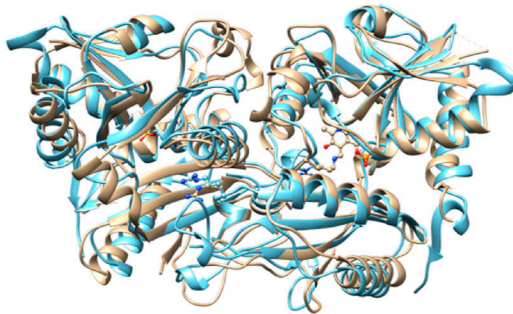
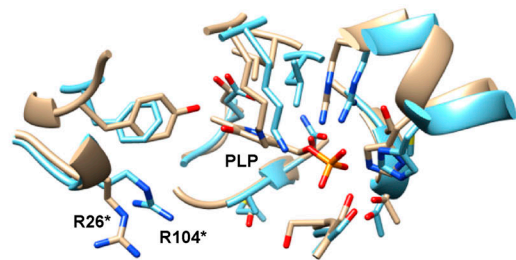
B**C**

Figure S2. Sequence alignment of Rv0812 with ADCL- and DAAT-like proteins from selected genomes. (A) ClustalW2 multisequence alignment of *Mtb* Rv0812-like sequences compared with ADCL- and DAAT-like sequences from *D. hafniense*, *P. aeruginosa*, *S. oneidensis*, *E. coli*, *V. cholerae*, *Streptomyces*, *A. bacterium*, *C. difficile*, *S. aureus*, *C. pusillum*, *A. thaliani*, *Desulfotalea*, *N. cyanobacterium*, *S. negevensis*, *G. endophyticus*, *Bacillus* YM-1, *L. sphaericus*, *L. monocytogenes*, *L. pneumophila*, *B. paraptusiss*, and *M. loti*. Sequences within the magenta box clustered along with Rv0812 in the phylogenetic tree, while known ADCL and DAAT sequences grouped with their respective subfamilies and are thus shown above and below Rv0812-like sequences, respectively. Residues conserved across all families are shown in red boxes. Conserved ADCL-like residues are shaded in blue, while DAAT-like residues are green and Rv0812-like residues are purple. **(B and C)** Superposition of Rv0812 (tan) and a homology model of *A. thaliana* ADCL/DAAT (blue). The ribbon diagram overlay, with the conserved Arg26* (Rv0812) and Arg104* (*A. thaliana* ADCL/DAAT) residues as ball and sticks, shows the structural similarity between the dually functional enzymes, with a 3.88-Å root-mean-square deviation between all atoms (B). A closer view of the residues within 4 Å of PLP demonstrates the high degree of similarity between the two active sites (C).

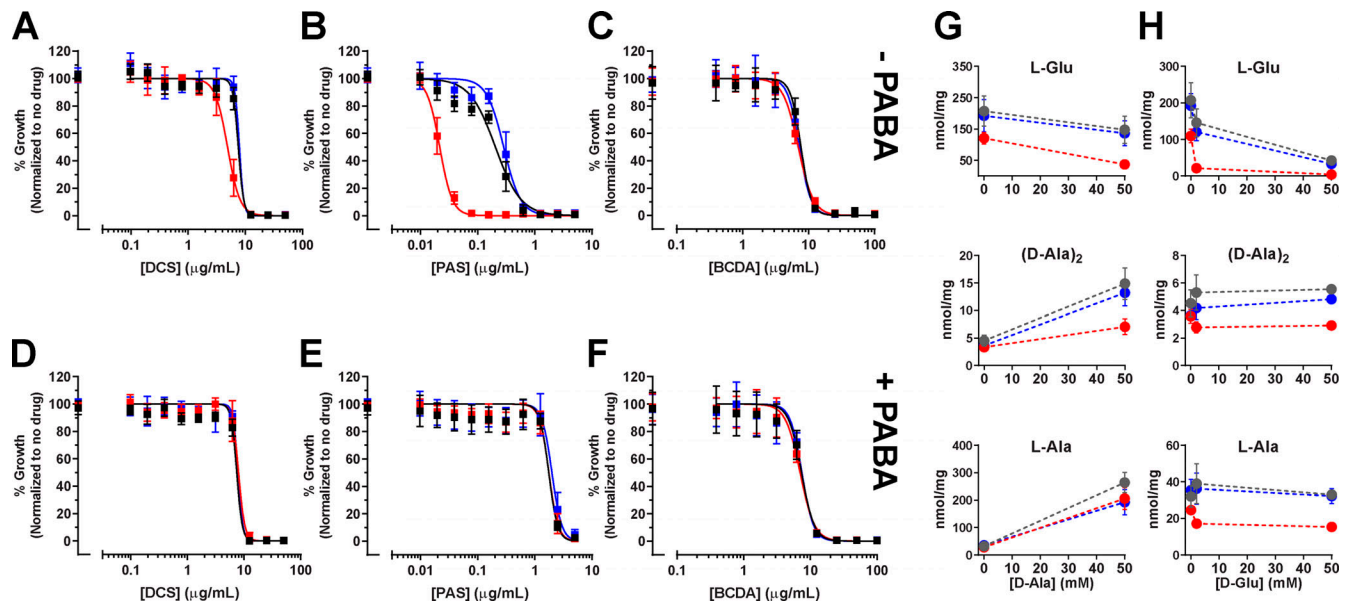


Figure S3. ***Mtb* $\Delta Rv0812$ is hypersusceptible to PAS, not DCS or BCDA.** (A–F) The minimum inhibitory concentrations of DCS (A and D), PAS (B and E), and BCDA (C and F) against *Mtb* WT (black), $\Delta Rv0812$ (red), and $\Delta Rv0812::Rv0812$ (blue) were determined in the absence (A–C) or presence (D–F) of PABA (1 μ g/ml). Cultures grown to mid-log phase were diluted into fresh Sauton's media to a starting OD_{580 nm} of 0.01 and OD was measured after 10 d. MIC₉₀ represents the drug concentration allowing 10% of maximum growth. No significant change in MIC of DCS or BCDA was observed across strains, independent of PABA supplementation (MIC₉₀ = 8.5–10 μ g/ml for DCS and 15 μ g/ml for BCDA). However, *Mtb* $\Delta Rv0812$ was hypersusceptible to PAS (MIC₉₀ = 0.03 μ g/ml) compared with WT and $\Delta Rv0812::Rv0812$ strains (MIC₉₀ = 0.6 μ g/ml), which was recovered by PABA supplementation (MIC₉₀ = 3 μ g/ml). SDs were obtained from at least two independent experiments. (G and H) Intracellular concentrations of metabolites from D-amino acid metabolism are shown in response to supplementation with 0, 2, and 50 mM D-Ala (G) or D-Glu (H). Intracellular metabolites from WT *Mtb* are shown in gray, while metabolites within $\Delta Rv0812$ and $\Delta Rv0812::Rv0812$ are shown in red and blue, respectively. SDs were obtained from at least two independent experiments.

Table S1 is provided online and lists detailed parameters of the crystallography data and refinement statistic.